CHALMERS
UNIVERSITY OF TECHNOLOGY

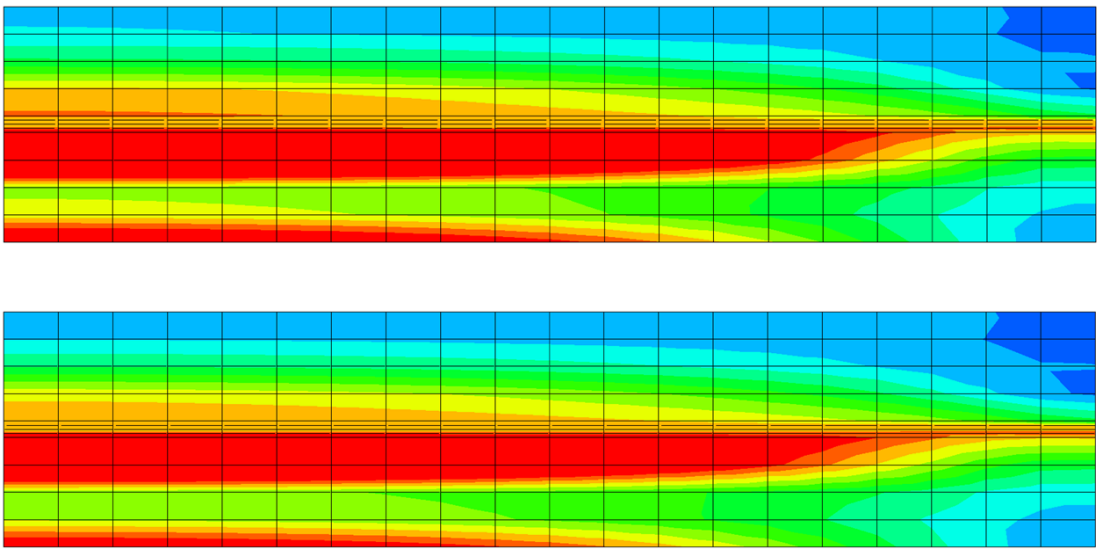

Implementation of a Material Model for Adhesives in Abaqus

Master's Thesis in Applied Mechanics

ROBIN AALTO
DANIEL KÄLL

DEPARTMENT OF INDUSTRIAL AND MATERIALS SCIENCE
CHALMERS UNIVERSITY OF TECHNOLOGY
Gothenburg, Sweden 2022
www.chalmers.se

Master's thesis 2022

Implementation of a Material Model for Adhesives in Abaqus

ROBIN AALTO
DANIEL KÄLL

CHALMERS
UNIVERSITY OF TECHNOLOGY

Department of Industrial and Materials Science
Division of Material and Computational Mechanics
Chalmers University of Technology
Gothenburg, Sweden 2022

Implementation of a Material Model for Adhesives in Abaqus
ROBIN AALTO
DANIEL KÄLL

Supervisor: Sandeep Shetty, Volvo Cars
Examiner: Martin Fagerström, Department of Industrial and Materials Science

Master's Thesis 2022
Department of Industrial and Materials Science
Division of Material and Computational Mechanics
Chalmers University of Technology
SE-412 96 Gothenburg
Telephone +46 31 772 1000

Cover: Stress distribution in a Bi-Metal Strip during curing of adhesive in Abaqus: Top, LS-DYNA: Bottom.

Typeset in LaTeX
Printed by Chalmers Reproservice
Gothenburg, Sweden 2022

Implementation of a Material Model for Adhesives in Abaqus
ROBIN AALTO & DANIEL KÄLL
Department of Industrial and Materials Science
Chalmers University of Technology

Abstract

In recent years it has become more common to use adhesive bonded multi-material structures in the automotive industry. These structures are however prone to distortions during the Electrocoat-oven process. These distortions are partly generated due to the curing of the adhesive, in combination with different coefficients of thermal expansion of the materials joined together ($\Delta\alpha$). One way to predict these distortions is through FE-simulation.

To be able to get accurate results from FE-simulations, a material model that accurately describes the degree of cure and its impact on the mechanical behaviour is required. Volvo Cars is therefore part of the research project MADBOND, in which a material model for adhesives has been developed and implemented in the FE-solver LS-DYNA.

In this master's thesis, the adhesive material model developed in the MADBOND project has been implemented as a user material model in the FE-solver Abaqus, which is the preferred solver for $\Delta\alpha$-simulations at Volvo Cars.

The Abaqus implementation was evaluated against both the existing implementation in LS-DYNA and a physical test.

In the evaluation, the results from Abaqus were within the defined error tolerance of 10% for the residual stresses and residual deformations, when compared to LS-DYNA. In the comparison with the physical test, the same buckling behaviour was noted in the results from both the Abaqus simulation and the test. Significant differences in the magnitudes of the residual displacements was however seen, which in some regions was 10 times larger in the test case. The differences were to a large extent explained by adhesive failure in the test, which was an aspect not included in the simulation model.

A convergence study was conducted for the material model, and it showed that the time increment size had a significant impact on the results, both in LS-DYNA and Abaqus. It was also discovered that the Abaqus implementation was not compatible with parallel execution. It was therefore recommended that these aspects are taken into consideration in any future work at Volvo Cars in order to perform accurate $\Delta\alpha$-simulations for large structures.

Keywords: Multi-Material Structures, Adhesive, $\Delta\alpha$, UMAT, Abaqus, LS-DYNA, CAE, FEA

Acknowledgements

A lot of people have been involved in the work conducted in this thesis, and it is unfortunately not possible to acknowledge everyone here.

With that said, we first and foremost want to thank our supervisor Sandeep Shetty at Volvo Cars, who has supported us throughout the entire thesis with his great dedication.

We also want to thank our examiner Martin Fagerström who has guided us through the work.

Furthermore, we would like to express our gratitude to Sibin Saseendran and Daniel Berglund at RISE. Without their dedicated support, none of the work in the thesis would have been possible.

Last but not least, we want to thank Renaud Gutkin and Marcus Schmidt at Volvo Cars, as both have shown great interest in our work and given us valuable feedback.

Robin Aalto & Daniel Käll, Gothenburg, May 2022

Contents

List of Figures

List of Tables

1

Introduction

1.1 Background

In the automotive industry, the time to market has been significantly reduced in recent years [1]. Simulation-based design processes play a vital role in reducing the product development cycle time. To cope with weight reduction and to meet increased safety requirements, the usage of a multi-material mix including aluminum alloys combined with high-strength steel has increased in automotive body structures in recent years. When a mixed material structure goes through an oven, there is a risk of permanent deformation of the parts due to different coefficients of thermal expansion (CTE) of the materials. This opens up for one of the significant issues with multi-material design, the $\Delta\alpha$-problem [2], which is the problem of combining materials with different coefficients of thermal expansion.

To be able to keep up with the short time to market, simulation-based design processes play a crucial role in reducing the product development cycle time. CAE-analysis gives the possibility to identify possible distortions from the manufacturing process when using materials with different thermal properties early in the development, which also means that the problems can be rectified at an early stage. To be able to use CAE-analysis, it is crucial that an accurate finite element (FE) model can be established. This accuracy is dependent on aspects such that the CAD-models that are imported into the FE pre-processor are geometrically correct and that a fine enough mesh is used, but also that the material models in the FE-software are accurate representations of the actual materials.

The existing adhesive material models which are used at Volvo Cars are not accurate enough for all manufacturing process simulations. One such scenario is the ED-oven process, in which the electrocoat applied to the car body cures. In this process, the adhesive applied throughout the car will also cure. As the adhesive cures, its mechanical properties will evolve until the final cured state is reached. At Volvo Cars there has been an increased interest in simulating these kind of processes, although the accuracy of these simulations has been restricted due to a lack of implemented material models in the FE-environment.

In order to solve the issues mentioned in the previous paragraph, Volvo Cars, along with other industrial partners, initiated the MADBOND project in 2020. The main purpose of project is to capture the impact of $\Delta\alpha$ (deviation in thermal expansion), that result in deformation in the adhesive joint after curing. The project aims to develop a physical model in a tool that can be used to predict the properties and quality of the adhesive joint.

From the MADBOND project, a material model for adhesives has been established [3], and it has also been implemented into the FE-solver LS-DYNA. However, the preferred FE-solver for implicit durability simulations (where $\Delta\alpha$-simulations are of interest) at Volvo Cars is Abaqus, and there is still no implementation of the developed material model in this FE-solver.

1.2 Aim

The aim of the thesis is to implement the adhesive material model, developed by the MADBOND-partner RISE, in Abaqus. The implementation will be verified by ensuring that the Abaqus implementation give numerical results for the residual stress and residual displacement, that are within 10% of the results from the LS-DYNA implementation. Furthermore, there should also be a correlation with the measured residual displacement from a physical component test.

1.3 Limitations

Due to constraints on the duration of the thesis, some limitations on the scope have been established.

The first of these is that the code for the implementation of the material model will not be written from scratch. It will rather be based on the existing implementation in LS-DYNA. The work in this thesis will therefore be a continuation of the work performed in the MADBOND project.

A further limitation is that the material model implemented in Abaqus shall be a direct implementation of the model developed in the MADBOND project. There will be no effort to improve the current material model, only to replicate it in Abaqus.

2

Theory

FEICA, the Association of the European Adhesive & Sealant Industry, provides the definition: "An adhesive can be defined as a substance that causes two surfaces to stick together"[4]. The term adhesives is thereby very wide, and different adhesives and types of adhesive, have different properties and characteristics.

The adhesive of interest at Volvo Cars for the specific application is a single-component epoxy hybrid structural adhesive. This chapter will therefore account for the theory relevant for the adhesive in question.

2.1 Epoxy Adhesives

Epoxy adhesives are one of the strongest types of adhesives available and therefore often used when structural, load-bearing, properties are sought [5]. Other properties of epoxy adhesives that are desired are their ability to adhere to many different types of surfaces, as well as their good chemical, thermal and water resistance [6].

Epoxy resins are a part of the family thermosetting polymers, which are characterized by that they go through an irreversible curing process that alters their properties [7].

2.1.1 General Theory of Epoxy

The most simple epoxy adhesives consist of only an epoxy resin mixed with a hardener. When the epoxy resin and hardener are mixed, a chemical reaction starts. This is a polymerization reaction in which the epoxy resin and hardener create a three-dimensional network through cross-linking, thus resulting in the rigidity and strength of the epoxy. This process is also what is commonly known as curing [6, 8]. The polymerization reaction is furthermore exothermic, meaning that it generates heat [9]. The heat generated from the exothermic reaction is dependent on the amount of epoxy resin cured at once. Since the adhesive lines are very thin, the exothermic reaction is unlikely to be problematic. For other applications when larger quantities of epoxy are involved, such as CFRP (Carbon-Fibre-Reinforced Polymers), the exothermic reaction can however generate a substantial amount of

heat that can cause damage to either the epoxy itself or the adherends that the epoxy is applied to [9, 10].

Epoxy adhesives are available in two different configurations, either as a two component system or a single component system.

2.1.2 Two Component Epoxy Adhesives

In the two component system, the resin and the hardener are stored separately and then mixed when they are applied. When mixing the resin and the hardener, the polymerization reaction starts and the adhesive starts curing. During application, the mix must be performed according to the ratio stated by the manufacturer. The mix can either be performed manually or by using a dispenser that automatically supplies the correct ratio.

Using the wrong ratios could result in the adhesive not curing sufficiently, the adhesive having a too low rate of cure, or the adhesive having a too high rate of cure, which could lead to an exothermic reaction with too large heat generation [11]. Two component epoxy systems generally have a tensile strength in the range of 20-30 N/mm^2 [5].

The benefits of a two component system is its long shelf life, and its lower sensitivity to environmental factors when compared to single-component systems [12], as two component systems can be stored in temperatures of 20 - 25 °C [13]. With that said, in products where the user mixes the two components at the time of application, there is a risk of inconsistent results. This problem is however solved to a large extent through the use of automatic dispensers [12].

2.1.3 Single-Component Epoxy Adhesives

A single component epoxy adhesive system also contains the two components resin and hardener, but these are already mixed when the user receives them. This is commonly made possible in one of two ways; mixing a two component system and then freezing it, thus stopping the polymerization until the adhesive is brought back to room temperature, or by utilizing latent hardeners that remain inactive until a certain temperature is reached [14, 15].

When latent hardeners are used, requirements on curing temperature and time are specified by the supplier. Diverging from these specifications can result in the adhesive not curing sufficiently. Single component epoxy adhesive systems generally have a tensile strength in the range of 35-41 N/mm^2 [5].

The benefits of a single component system is its superior strength compared to two component systems, it also has higher thermal resistance compared to two component systems [16]. Single component systems however need to be handled with greater care than two-component systems. Pre-mixed two-component systems need to be stored at a temperature of -40 °C, and once they have been brought

to room temperature they can not be frozen again [13]. Single component systems with latent hardeners are not as sensitive to temperature, although they still need to be kept at a temperature of 5-10 °C to prevent premature curing [13].

2.1.4 Modifying Epoxy Adhesives

Epoxy adhesives can be modified by utilizing fillers and additives. These fillers and additives can alter the properties and appearance of the epoxy resin and can thereby make them more suitable for certain applications [17]. For example, the viscosity of the uncured epoxy can be increased with fillers, thus making it more suitable for applications on vertical surfaces as it prevents the resin from running off.

Furthermore, the epoxy resin can be combined with other polymeric resins to create epoxy-hybrid resins. Example of epoxy-hybrids are epoxy-urethane and epoxy-polysulfide [18]. This allows the properties of the epoxy to be modified, for example making it more flexible.

2.2 Material Behaviour of Adhesives

Adhesives, and specifically epoxy adhesives, are polymeric materials and thus in large have viscoelastic behaviour [19]. There are however publications that argue that adhesives in a fully cured state can accurately be described as having an elastic behaviour [20, 21].

With that said, since the material behavior of interest at Volvo Cars is that during curing, the viscoelastic response must be considered. Furthermore, assuming elastic properties for a cured adhesive would imply that the adhesive reaches 100% cure, whilst in practice the final degree of cure can generally be expected to be in the range 90-100% [22].

2.2.1 Curing

The degree of cure (DoC) α is a measurement of how much an adhesive (or other thermosetting polymer) has cured [22]. It can described as a fraction in the range 0 to 1, where 0 indicates a completely uncured adhesive in viscous liquid form and 1 a completely cured adhesive as a solid.

When the adhesive goes through the curing process, it goes through several phase changes [23]. In the start of the process, as the adhesive is uncured ($\alpha = 0$), it has the properties of a viscous liquid, which allows it to be applied to the adherends. As the curing progresses towards the gel point, which often lies in the interval $\alpha = 0.4 - 0.6$, the adhesive becomes more and more viscous. When it reaches the gel point, it has transformed from a liquid state to a gelled state, where the adhesive behaves as a semi-solid gel material [22].

As the curing proceeds further, there is also an increase in the glass transition temperature. When the glass transition temperature has increased to the point

where it is equal to the applied temperature in the curing cycle, vitrification occurs. The vitrification means that the adhesive will behave like a solid as it inherits a glassy state.

During the curing cycle there will also be volumetric changes to the adhesive. These volumetric changes are namely thermal expansion and chemical shrinkage.

2.2.1.1 Kamal model

One model that is often used to calculate the degree of cure is the Kamal model [24].

In the Kamal model, the rate of cure is calculated using Equation (2.1)

$$\frac{\mathrm{d}\alpha}{\mathrm{d}t} = (k_1 + k_2\alpha^m)\,(1-\alpha)^n\,, \tag{2.1}$$

where the Arrhenius constants k_1 and k_2 are calculated as

$$k_i = A_i \exp\left(-\frac{E_i}{RT}\right), \tag{2.2}$$

and where A_i and E_i are material constants, R is the ideal gas constant, and T is the temperature.

The exponent n in the Kamal equation is furthermore calculated as

$$n = n_a + n_b T, \tag{2.3}$$

where n_a and n_b are material constants and T is the temperature.

2.2.2 Chemical Shrinkage

When a thermosetting polymer, such as an epoxy resin, cures, the volume will change with the temperature due to thermal expansion or thermal contraction. The other aspect that will influence the volumetric change in the thermosetting polymer is chemical shrinkage. The chemical shrinkage occurs due to the cross-linking of polymer chains in the material during the polymerization reaction. During this reaction, the density of the thermosetting polymer increases, which in turn leads to a decrease of volume [25, 26].

The curing cycle can be divided in to three phases; heating, constant temperature and cooling. During the second phase of the curing, when the temperature is held constant, the chemical shrinkage occurs [27].

According to [28] the chemical shrinkage can be neglected, due to it not having a large affect in comparison to the thermal deformations, for the residual stresses. There are however other studies that have shown that the chemical shrinkage does have a greater affect than earlier anticipated [29], showing that it is causing a significant portion of the distortion before the cooling phase of the curing process [26].

2.2.3 Stress Relaxation and Creep

A viscoelastic material is characterized by the fact that the stress-strain response of the material exhibits both viscous and elastic behaviour [30]. The elastic stress response is purely dependent on the applied strain, whilst the viscous portion of the response is dependent on strain rate and time. This is illustrated in Figure 2.1, where it can be seen that the stress in the material decreases with time as the strain is held constant, this phenomena is known as stress relaxation [31].

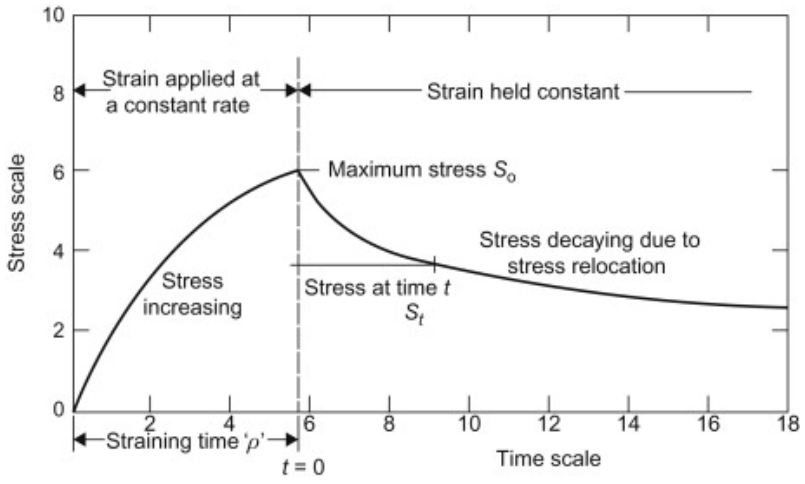

Figure 2.1: Stress curve during constant strain for a viscoelastic material [31].

Another phenomena exhibited by viscoelastic materials is creep. This phenomena is apparent when a stress is held constant in the material, which leads to an increase in strain over time [32]. This behaviour is illustrated in Figure 2.2.

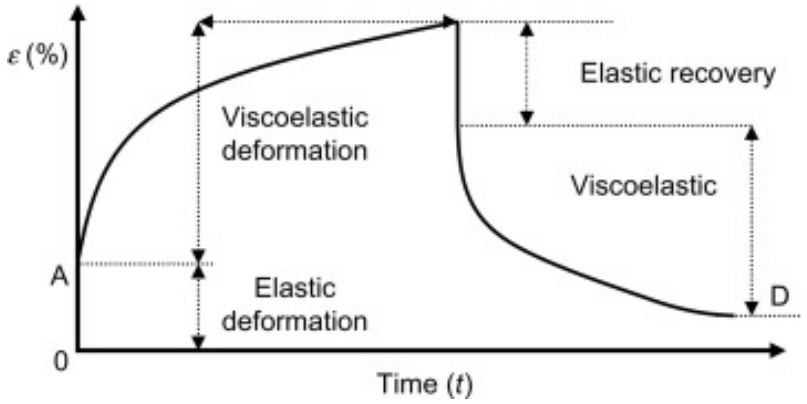

Figure 2.2: Strain curve during constant stress for a viscoelastic material [32].

2.2.3.1 Prony Series

The relaxation behaviour of viscoelastic material can be expressed as a Prony series, with the Prony terms G_i and the relaxation times τ_i

$$G(t) = G_\infty + \sum_i G_i e^{-t/\tau_i}, \tag{2.4}$$

where $G(t)$ is the stress relaxation modulus with respect to the time t, G_∞ is the stress relaxation modulus as $t \to \infty$, and i is the number of Prony terms [33]. A Prony series with a larger number of terms will give a more accurate representation of the relaxation behaviour in the material.

The values for G_i and τ_i can be obtained through testing of the material using Dynamic-Mechanical Analysis (DMA)/ Dynamic-Mechanical Thermal Analysis (DMTA) [34]. The testing is performed in a test rig that applies a sinusoidal force with a frequency ω at a temperature T, which induces a stress state in the material, from which the strain in the material is recorded [35].

The storage modulus G' can be expressed with respect to the frequency ω as

$$G'(\omega) = G_\infty + \sum_i \frac{G_i \omega^2 \tau_i^2}{1 + \omega^2 \tau_i^2}. \tag{2.5}$$

The loss modulus G'' can in the same manner be expressed as

$$G''(\omega) = \sum_i \frac{G_i \omega \tau_i}{1 + \omega^2 \tau_i^2}. \tag{2.6}$$

The results from the DMA/DMTA test can be be fitted to either Equation (2.5) or (2.6), in order to obtain the values for G_i and τ_i. With that said, the testing should be conducted at a wider range of frequencies if the equation for the loss modulus G'' is to be used, since the magnitude is significantly lower than for the storage modulus G' [33].

The viscoelastic relaxation of a material is often defined in FE-software as Prony series in tabular form, which include the relaxation times τ_i as well as the dimensionless values g_i for the relaxation moduli [36]. The dimensionless values for the relaxation moduli g_i can be obtained as

$$g_i = \frac{G_i}{G_0}, \tag{2.7}$$

where G_0 is the value of $G(t)$ as $t = 0$.

2.2.4 Temperature Influence

As an adhesive is placed in an oven to cure, it will experience temperatures in the range of 20 - 200 °C. This will not only cure the adhesive but also influence the overall behavior of the adhesive. The behavior of a viscoelastic polymer can be defined in five temperature-dependent regions [37], these regions are:

1. Glassy region
2. Glass transition region
3. Rubbery region
4. Rubbery flow region
5. Liquid flow region

These regions are furthermore illustrated in Figure 2.3.

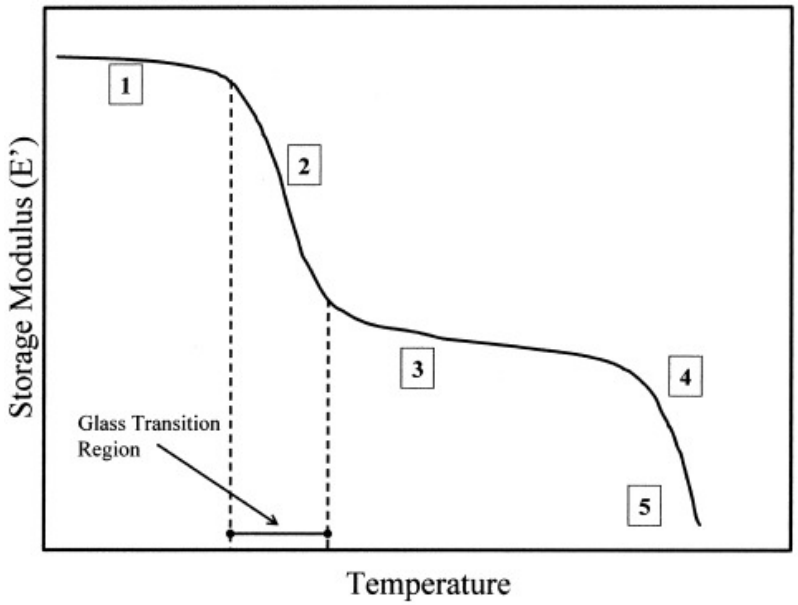

Figure 2.3: Temperature influence on storage modulus [37].

As seen in Figure 2.3, an increase in temperature will result in a lower modulus. With that said, since the stress-strain response of a viscoelastic material is also time-dependent, the temperature cannot simply be accounted for by modifying the modulus of the material. It can however be achieved by time-temperature superposition through the introduction of a shift function [38].

The curing of the adhesive introduces another aspect of the temperature dependency, since the glass transition temperature evolves during curing. Which means that the glass transition temperature T_g can be defined as a function of the degree of cure α as $T_g(\alpha)$. As illustrated in Figure 2.3, the stress in the material is dependent on the

temperature, and also the glass transition temperature, which consequently leads to the modulus being a function of both temperature and degree of cure as $E(T, \alpha)$.

2.2.4.1 Shift Function

As a polymeric material is subjected to increased temperatures, the relaxation times in the stress response for the material become shorter [39]. Figure 2.4 illustrates how this behavior may look when experimentally recorded for an arbitrary material that exhibits viscoelastic behaviour.

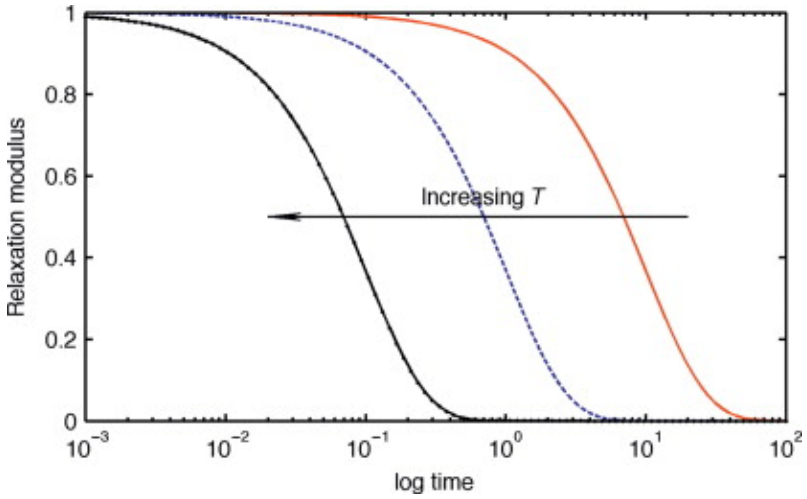

Figure 2.4: Relaxation modulus at different temperatures [39].

In Figure 2.4, it can be noted that the behaviour essentially is the same for the different temperatures, although shifted in time. This indicates that the temperature influence can accurately be accounted for by a shift factor. It is however important to note that this is only true for thermorheologically simple materials [39]. For thermorheologically complex materials, the relaxation at different temperatures exhibit more significant differences that cannot be accounted for with a shift function.

The shift in time illustrated in Figure 2.4 can be expressed as

$$\log a_T = \log t_{T_{\text{ref}}} - \log t_T, \tag{2.8}$$

where $t_{T_{\text{ref}}}$ is the time at the temperature T_{ref} and t_T is the time at the temperature T.

Following Equation (2.8), it can be concluded that the relaxation behavior can be accounted for by time-temperature superposition by a shift factor $a_T(T)$.

With that said, the introduction of a shift factor relies on the existence of a master curve, which has to be constructed initially [39]. The master curve defines the

relaxation behavior at the temperature T_{ref} and is used as a reference. The master curve can be determined through DMA testing [40].

There are several approaches for determining the shift factor, but two of the most commonly used are the WLF (Williams, Landel & Ferry) equation and the Arrhenius equation [41].

The WLF equation defines the time shift factor a_T as

$$\log a_T(T) = \frac{-C_1(T - T_{\text{ref}})}{C_2 + (T - T_{\text{ref}})}, \tag{2.9}$$

where C_1 and C_2 are material constants that can be fitted to the test data, T is the temperature, and T_{ref} is the reference temperature at which the test was performed.

The Arrhenius equation on the other hand defines the shift factor as

$$\ln a_T(T) = -\frac{E_a}{R}\left(\frac{1}{T} - \frac{1}{T_{\text{ref}}}\right), \tag{2.10}$$

in which E_a is the activation energy, R is the universal gas constant, T is the temperature, and T_{ref} is the reference temperature [42].

For better comparison, Equation (2.10) can be written in the same 10-base logarithm as Equation (2.8) and (2.9)

$$\log a_T(T) = -\frac{E_a}{2.303R}\left(\frac{1}{T} - \frac{1}{T_{\text{ref}}}\right). \tag{2.11}$$

It is generally accepted that the shift factor calculated using the WLF equation is more accurate for temperatures above the glass transition temperature, whilst the Arrhenius equation is more accurate for temperatures below the glass transition temperature [43].

2.3 Implicit and Explicit Time Integration

Explicit and implicit time integration are often used for numerical analysis to solve time-dependent ODEs (ordinary differential equations) and partial differential equations, for both dynamic and static cases. These two methods are both used in LS-DYNA and Abaqus, to solve numerical problems.

The implicit time integration is unconditionally stable, meaning that the increment size decrease automatically until the solution for the increment is stable. The explicit integration is on the other hand conditionally stable, which means that it needs sufficiently small time steps to obtain a stable solution.

Implicit integration is preferable for quasi-static simulations with small deformations, while explicit integration is better suited for rapid simulations with large deformations, such as car crashes and ballistic explosions [44].

The advantage of using an implicit solution is that the number of time steps can be significantly fewer compared to the explicit solution. The time to reach convergence for the implicit solution can however vary depending on the size and amount of time steps, which could increase the computational time [45].

A second-order differential equation at the time step $n + 1$, can be described with Equation (2.12)

$$\boldsymbol{M}\ddot{\boldsymbol{u}}_{n+1} + \boldsymbol{C}_{n+1}\dot{\boldsymbol{u}}_{n+1} + \boldsymbol{K}_{n+1}\boldsymbol{u}_{n+1} = \boldsymbol{P}_{n+1}, \tag{2.12}$$

where $\ddot{\boldsymbol{u}}_{n+1}$, $\dot{\boldsymbol{u}}_{n+1}$ and $\boldsymbol{u}_{n+1}$ are the acceleration, velocity and displacement respectively, and $\boldsymbol{M}$, $\boldsymbol{C}$ and $\boldsymbol{K}$, are the mass matrix, the damping coefficient and stiffness matrix respectively, with n being the current time step.

The implicit time integration can from this be described with the Newmark method, which is a method of numerical integration used to solve certain differential equations, that gives a relation to how the acceleration at the end of the increment affects the velocity and displacement.

The first and 0^{th} order derivative can be described with Equations (2.13) and (2.14) respectively

$$\dot{\boldsymbol{u}}_{n+1} = \dot{\boldsymbol{u}}_n + \frac{\Delta t}{2}(\ddot{\boldsymbol{u}}_n + \ddot{\boldsymbol{u}}_{n+1}), \tag{2.13}$$

$$\boldsymbol{u}_{n+1} = \boldsymbol{u}_n + \Delta t\dot{\boldsymbol{u}}_n + \frac{1-2\beta}{2}\Delta t^2\ddot{\boldsymbol{u}}_n + \beta\Delta t^2\ddot{\boldsymbol{u}}_{n+1}, \tag{2.14}$$

where β is a constant in the range of 0 to 1. The value of $\beta = 0.25$ is commonly used, which results in the constant acceleration method.

The Newmark method can also be written as an explicit time integration by using $\beta = 0$ [46].

3

Literature Survey - Adhesive Material Models

In this chapter, a general literature study on available material models is presented. This includes what physical aspects that have been included in each model, and when sufficient information was available, how the physical aspects have been modeled.

3.1 RISE/MADBOND Material Model

The material model that has been developed by RISE, and that is now also a part of the MADBOND project was presented in its one-dimensional form in [3]. The constitutive equations for the full 3D model, the LS-DYNA implementation, as well as further information regarding the model, were obtained through direct communication with the authors Sibin Saseendran and Daniel Berglund at RISE.

The material model was originally developed for CFRP (Carbon-fiber-reinforced polymers), but since both the matrix in the CFRP and the structural adhesives of interest consist of epoxy, the material model can with some minor modifications also be used for adhesives. These modifications mainly show in the material data input, where the adhesive has isotropic material properties as opposed to the CFRP that has anisotropic material properties.

One difference in the material model itself between the adhesive and the CFRP is that the exothermic reaction is neglected for the adhesive. The reasoning behind this is that the thickness of the bond lines for the adhesive is small (< 0.5 mm), and the heat generated from the adhesive is therefore negligible. The thickness of CFRP is on the other hand in many applications considerably larger, thus resulting in a larger amount of generated heat.

The material model is a viscoelastic model with complex rheological behavior, which accounts for the rubbery and glassy modulus dependent on degree of cure and temperature. The model is based on three functions dependent on both the temperature and the degree of cure; the rubbery modulus $E_r(\alpha, T)$, the weight factor $h_1(\alpha, T)$, and $h_2(\alpha, T)$ defining how the strain affects the loading history [3].

To give a basic explanation, the 1D case of the viscoelastic model is shown in Equations (3.1)-(3.9).

In the following equations, the implicit increment of an arbitrary variable $f(t)$ is denoted as $\Delta f^{k+1} = f(t_{k+1}) - f(t_k)$, and its derivative as $d_f^{k+1} = \frac{f^{k+1}-f^k}{t_{k+1}-t_k}$.

For a small time increment Δt_{k+1}, the shift factor a, the strain ϵ, and h_2, are assumed to be linear functions of time τ. The shift factor a is present as the product of the temperature and DoC

$$a = a^k + d_a^{k+1}(\tau - t_k) \tag{3.1}$$

assuming that $h_2(\alpha, T)$ and ϵ have linear dependence of time τ in the interval $[t_k, t_{k+1}]$

$$h_2(\tau) = h_2(t_k - 0) + d_{h2}^{k+1}(\tau - t_k)H(\tau - t_k) \tag{3.2}$$

$$\epsilon(\tau) = \epsilon(t_k - 0) + d_\epsilon^{k+1}(\tau - t_k)H(\tau - t_k) \tag{3.3}$$

where H is the Heaviside step function.

With the assumption of linear change of the shift factor a over the increment, together with the assumption $\ln(1 + x) \approx x$, the increment of the reduced time ψ can be seen in Equation (3.4)

$$\Delta\psi_{k+1} = \frac{\Delta t_{k+1}}{a^{k+1}}\left(1 - \frac{1}{2}\frac{\Delta a^{k+1}}{a^k}\right). \tag{3.4}$$

The explicit stress increment can be seen in Equation (3.5), for a given strain ϵ, temperature T and degree of cure α.

$$\Delta\sigma^{k+1} = \Delta E_r^{k+1}\epsilon^k + E_r^{k+1}\Delta\epsilon^{k+1} + \sum_i C^i S_i^k\left(h_1^{k+1}\exp\left(-\frac{\Delta\psi_{k+1}}{\tau_i}\right) - h_1^k\right) + h_1^{k+1}\sum_i C^i\Delta\Theta_i^{k+1} \tag{3.5}$$

In Equation (3.5), C^i denotes the Prony series constants, and τ_i the corresponding relaxation times. The material model can be used with a Prony series with up to 9 terms.

The integrations $\Delta\Theta_i^{k+1}$ and S_i^k in Equation (3.5) are defined in Equation (3.6) and (3.7)

$$\Delta\Theta_i^{k+1} = [h_2^k \Delta\epsilon^{k+1} + h_1^{k+1}\epsilon^k]\Delta\hat{I}_i^{k+1} + 2\Delta h_2^{k+1}\Delta\epsilon^{k+1}\Delta\hat{N}_i^{k+1} \tag{3.6}$$

$$S_i^k = S_i^{k+1}\exp\left(-\frac{\Delta\psi_k}{\tau_i}\right) + \Delta\Theta_i^k. \tag{3.7}$$

The integrations $\Delta\hat{I}_i^k$ and $\Delta\hat{N}_i^k$ in Equation (3.6) are defined in Equation (3.8) and (3.9)

$$\Delta\hat{I}_i^k = \frac{1}{d_a^k + \frac{1}{\tau_i}}\left(d_a^k + \frac{1-\exp\left(-\frac{\Delta\psi_k}{\tau_i}\right)}{\frac{\Delta t_k}{a^{k-1}}}\right), \tag{3.8}$$

$$\Delta\hat{N}_i^k = \frac{1}{2d_a^k + \frac{1}{\tau_i}}\left(\frac{a^k}{\Delta t_k} - \frac{a^{k-1}}{\Delta t_k\left(d_a^k + \frac{1}{\tau_i}\right)}\frac{a^k - a^{k-1}\exp\left(-\frac{\Delta\psi_k}{\tau_i}\right)}{\Delta t_k}\right). \tag{3.9}$$

The material model presented above describes a thermorheologically complex adhesive. The model can however be simplified to a thermorheologically simple material model by introducing a rubbery modulus E_r that is independent of the temperature and DoC, and setting the VE-parameters $h_1 = h_2 = 1$ [3].

3.2 Priesnitz's Material Model

The PhD thesis "On local panel distortions due to hot-curing adhesives" [26], written by Konstantin Priesnitz, had as aim to investigate the local distortions that occur due to adhesive bonding. This also included developing a simulation model that could be used to predict these distortions. The model developed was based on tests also performed in the same thesis work.

The material model developed by Priesnitz includes the chemical shrinkage and thermal deformations as well as gelation and stress relaxation of a viscoelastic material. The cure cycle is divided in to three stages, which can be seen in Figure 3.1, with each stage described by different constitutive equations.

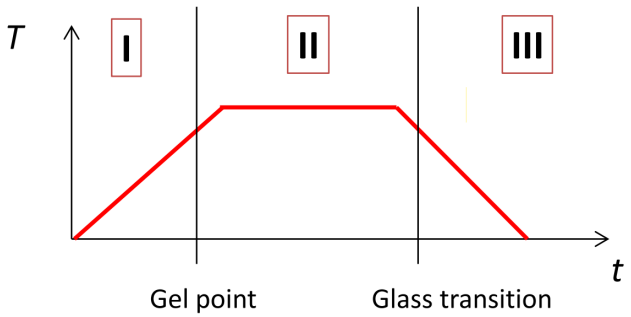

Figure 3.1: Stages describing material behaviour of Priesnitz material model.

3.2.1 Stage I

In stage I, before the gel point has been reached, the material is described as a viscoelastic liquid with the equilibrium shear modulus as zero. Therefore, the material cannot sustain any stresses or strains in this stage.

3.2.2 Stage II

Stage II describes the material behaviour after the gel point has been reached. In stage II the temperature is well above the glass transition temperature of the adhesive, which consequently leads to the mechanical behaviour of the material being dominated by the rubbery modulus. It is therefore assumed that any relaxation in the material can be neglected. Priesnitz argues that the material in this stage can be described with a temperature and degree of cure dependent elastic stress-strain relation.

3.2.3 Stage III

Stage III of the material model describes the material behaviour after the glass transition during cooling. In this stage, the material is considered to have viscoelastic behaviour with relaxation times that are dependent on temperature and degree of cure. The volumetric changes due to thermal expansion and chemical shrinkage and the resulting strains from these changes are calculated in the same way as in stage II.

The model furthermore includes two different CTE, one before and one after the glass transition temperature, α_r (rubbery CTE) and α_g (glassy CTE). A function $\alpha(T)$ is also introduced to smooth the transition between α_g and α_r.

3.2.4 Constitutive Equations

The material is assumed to be isotropic with deformations that can be described as the sum of the thermal, chemical and mechanical strain, seen in Equation (3.10)

$$\epsilon_{ij} = \epsilon_{ij}^{\mathrm{me}} + \epsilon_{ij}^{\mathrm{th}} + \epsilon_{ij}^{\mathrm{ch}}. \tag{3.10}$$

The rubbery CTE is defined as

$$\alpha_r = \frac{1}{3}(k_1 + k_2), \tag{3.11}$$

and the glassy CTE as

$$\alpha_g = \frac{1}{3}k_1, \tag{3.12}$$

with the transition between the two

$$\alpha(T) = \frac{1}{3}\left[k_1 + \frac{1}{2}k_2(1 + \tanh(C_0(T - T_g)))\right], \tag{3.13}$$

where k_1, k_2 and C_0 are material constants, T is the current temperature, and T_g the glass transition temperature.

The constitutive equations are obtained by splitting the stress tensor σ_{ij} into a deviatoric part and hydrostatic pressure p

$$\sigma_{ij} = \sigma_{ij}^{\mathrm{dev}} - p\delta_{ij}. \tag{3.14}$$

The volume changes in the model are described with the hypo-elastic Equation (3.15)

$$-\dot{p} = K\dot{\epsilon}_{kk}^{\mathrm{me}}, \tag{3.15}$$

with the bulk modulus calculated as

$$K = \frac{E_g}{3(1 - 2\nu)}, \tag{3.16}$$

and where E_g is the instantaneous glassy tensile modulus.

The shear behaviour of the model changes during the three different stages described previously. Because the adhesive can not exert permanent stresses or strains in stage I the shear modulus is set as very small, although not zero.

In stage II the deviatoric stress-strain relation is set as hypo-elastic

$$\dot{\sigma}_{ij}^{\mathrm{dev}} = 2G(\alpha)\dot{\epsilon}_{ij}^{\mathrm{me,dev}}, \tag{3.17}$$

with the shear modulus

$$G(q) = G^{\mathrm{final}} \left(\frac{q^2 - q_{\mathrm{gel}}^2}{1 - q_{\mathrm{gel}}^2} \right)^{\frac{8}{3}}, \tag{3.18}$$

and where q is the degree of cure and q_{gel} is the degree of cure at the gel point.

In stage III a linear viscoelastic material law is introduced in order to capture the relaxation behaviour in the material

$$\dot{\sigma}_{ij}^{\mathrm{dev}} = 2G_{\infty}\dot{\epsilon}_{ij}^{\mathrm{me,dev}} + 2\sum_{m=1}^{M} G_m \dot{u}_{ij}^{m}, \tag{3.19}$$

$$\dot{\epsilon}_{ij}^{\mathrm{me,dev}} = \dot{u}_{ij}^{m} + \frac{1}{a(T)\tau_m} u_{ij}^{m}, \quad m = 1, 2..., M. \tag{3.20}$$

The material behaviour is in this stage assumed to be thermorheologically simple, with a shift factor $\log a(T)$. The shear relaxation modulus at the reference temperature in stage III is calculated as

$$G(t) = G_{\infty} + \sum_{G_m} \exp\left(-\frac{t}{\tau_m} \right). \tag{3.21}$$

A quasi-static approach is utilized to obtain the shear modulus for temperatures other than the reference temperature

$$G(t) = \frac{3KE(t)}{9K - E(t)}. \tag{3.22}$$

3.3 LS-DYNA - MAT_277

MAT_277 (*MAT_ADHESIVE_VISCOELASTIC) is a default material model available in LS-DYNA. It is developed specifically for simulating adhesive materials during curing [47]. The curing kinematics in the material model follow the Kamal model and depends on temperature and temperature rate. The constitutive model is described as a general viscoelastic Maxwell model with relaxation that is defined as a Prony series with a maximum of 16 terms.

The material model considers chemical shrinkage (γ) depending on the degree of cure (α), which can either be specified by the user in tabular form, or by defining the parameters γ_2, γ_1 and γ_0 in the quadratic expression:

$$\gamma(\alpha) = \gamma_2\alpha^2 + \gamma_1\alpha + \gamma_0 \tag{3.23}$$

While defining the material in LS-DYNA, there are three available options for the user on how the material model should take the temperature influence on stress relaxation into account.

1. No temperature influence on stress relaxation.

2. Time-temperature superposition using a shift factor calculated with the WLF (Williams, Landel & Ferry) equation [48].

3. Time-temperature superposition using a shift factor calculated with the Arrhenius equation [49].

4

Method

The project was in large divided into two segments, the first of which being the implementation of the material model in Abaqus. The second segment was the verification of the implemented material model. The methodology for both the implementation and the verification will be described in this chapter.

4.1 Implementation of Material Model in Abaqus

The material model developed by RISE was implemented in the FE software Abaqus as a UMAT (user material model). The UMAT was written in the language Fortran, which is one of the languages accepted by Abaqus, along with C and C++.

The constitutive equations describing the material behavior had previously been implemented in a subroutine by RISE. The implementation developed in this project was therefore not written from scratch, but was rather based on the previous implementation. With that said, due to concerns regarding confidentiality, the source code for the subroutine was not obtained from RISE, instead the subroutine was obtained as a pre-compiled object file (.o). This objective file can be seen as a "black box" where the contents can not be seen.

Since the constitutive equations had already been implemented, the purpose of the UMAT code developed in this project was to wrap the obtained object file, in what can be seen as "bridge" between Abaqus and the general constitutive equations. The reason for this is that Abaqus cannot communicate directly with the subroutine written by RISE, and the code developed in this project therefore acts as an intermediate step. This intermediate step arranges the inputs and outputs from both Abaqus and the material model subroutine in such a way that they can communicate with each other.

The material parameters are defined in the Abaqus input file, which is then passed into the UMAT subroutine. During calculations, the UMAT is called for every integration point in the adhesive, which, in turn, calls the pre-compiled subroutine located inside the object file. From the calls to the object file, the UMAT subroutine obtains the updated stresses and material state, which it in turn sends back to Abaqus. These interactions are also illustrated in Figure 4.1.

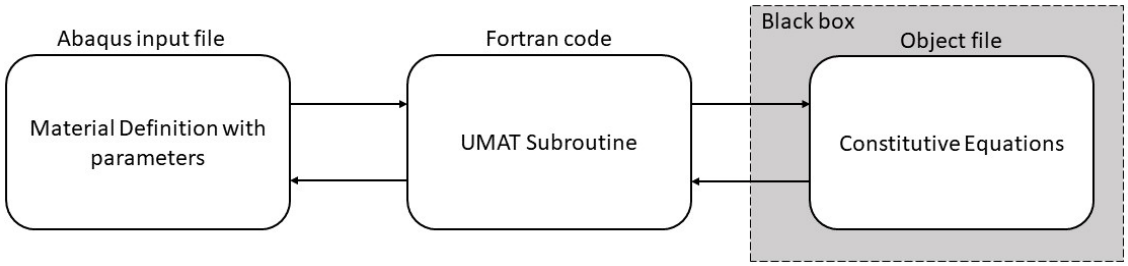

Figure 4.1: Interactions between the different routines.

4.1.1 RISE subroutine

As previously stated, the subroutine that implements the constitutive equations for the material was obtained as a pre-compiled object file from RISE. Therefore, the exact manner of the implementation is not known. The header of the subroutine is however required in order to be able to call it, and it was therefore also obtained from RISE. The header contains the name of the subroutine, which in this case is "umat42", as well as the input and output variables in the correct order. The header for the subroutine umat42 can be seen in Figure 4.2. Moreover, the input and output variables for the subroutine are disclosed in Table 4.1.

```
subroutine umat42(cm,eps,sig,hsv,dt1,time,
1           temper,cma,crvP,crvt)
```

Figure 4.2: Header for subroutine umat42, containing the constitutive equations.

Table 4.1: Variable in and output in umat42 subroutine.

Input	
Variable name	**Variable definition**
cm	Material constants
eps	Strain increment ($\Delta\varepsilon$) in Voight notation
dt1	Time increment (Δt)
time	Time at the start of the increment
temper	Temperature in the end of the increment
cma	Additional material constants
crvP	Prony series weights
crvt	Prony series relaxation times
Input & Output	
Variable name	**Variable definition**
hsv	History variables
Output	
Variable name	**Variable definition**
sig	Stress in Voight notation

There are a total of 20 material parameters in the cm array, and a total of 44 material parameters in the cma array. The material parameters are disclosed in full in Appendix A.

The subroutine furthermore utilizes 87 history variables for the material, with degree of cure, liquid fraction, solid fraction, and glass transition temperature being a few of them. The history variables are both an input and an output, as they get updated during the call to the routine. A full list of the history variables can be seen in appendix B.

The relaxation behaviour is, as disclosed in Section 3.1, accounted for by a Prony series. The Prony series is input into the subroutine as the variables crvP and crvt as one-dimensional arrays with a maximum of nine values.

4.1.2 Abaqus UMAT

The Abaqus UMAT was as previously stated, written in the language Fortran, and more specifically Fortran77 which requires fixed formatting.

The UMAT in Abaqus uses a standard header for the subroutine, which was obtained from the Abaqus manual, and can be seen in Figure 4.3.

```
      SUBROUTINE UMAT(STRESS,STATEV,DDSDDE,SSE,SPD,SCD,
     1 RPL,DDSDDT,DRPLDE,DRPLDT,
     2 STRAN,DSTRAN,TIME,DTIME,TEMP,DTEMP,PREDEF,DPRED,CMNAME,
     3 NDI,NSHR,NTENS,NSTATV,PROPS,NPROPS,COORDS,DROT,PNEWDT,
     4 CELENT,DFGRD0,DFGRD1,NOEL,NPT,LAYER,KSPT,JSTEP,KINC)
C
      INCLUDE 'ABA_PARAM.INC'
C
      CHARACTER*80 CMNAME
      DIMENSION STRESS(NTENS),STATEV(NSTATV),
     1 DDSDDE(NTENS,NTENS),DDSDDT(NTENS),DRPLDE(NTENS),
     2 STRAN(NTENS),DSTRAN(NTENS),TIME(2),PREDEF(1),DPRED(1),
     3 PROPS(NPROPS),COORDS(3),DROT(3,3),DFGRD0(3,3),DFGRD1(3,3),
     4 JSTEP(4)


      user coding to define DDSDDE, STRESS, STATEV, SSE, SPD, SCD
      and, if necessary, RPL, DDSDDT, DRPLDE, DRPLDT, PNEWDT


      RETURN
      END
```

Figure 4.3: Standard header for UMAT in Abaqus.

The standard header is the framework that was used when creating the UMAT subroutine. All the variables that are defined by Abaqus are listed in Appendix D,

however many of them are not used in this application, and therefore the variables of interest in this case are listed in Table 4.2.

Table 4.2: Used UMAT variables.

Input	
Variable name	**Variable definition**
STRAN	Strain in the start of the increment (ε)
DSTRAN	Mechanical strain increment ($\Delta\varepsilon_{mech.}$)
TIME	Time at the start of the increment
DTIME	Time increment (Δt)
TEMP	Temperature at the start of the increment
DTEMP	Increment of temperature (ΔT)
NSTATV	Number of solution-dependent state variables
PROPS	User-defined material constants
Input & Output	
Variable name	**Variable definition**
STRESS	Stress array
STATEV	Solution-dependent state variables
Output	
Variable name	**Variable definition**
DDSDDE	Jacobian matrix $\frac{\partial \Delta\sigma}{\partial \Delta\epsilon}$

The Fortran code that was written can be seen in Appendix C. It takes the stress, strain, and solution-dependent state variables at the start of the increment as input. Based on this input, the subroutine computes the updated stesses, the Jacobian $\frac{\partial \Delta\sigma}{\partial \Delta\epsilon}$, and the solution-dependent state variables at the end of the increment, and sends it back to Abaqus via the UMAT interface. The solution-dependent state variables (STATEV) in Abaqus correspond to the history variables (hsv) in the umat42 subroutine.

The Fortran code in Appendix C was compiled with Intel Fortran Compiler 17.2, with the options -fpic and -c, which resulted in an object file. This object file was then merged with the object file obtained from RISE using the GNU ar program with the -cr option.

4.2 Verification of Abaqus implementation

The implementation of the material model in Abaqus was verified with two test cases, where the results were compared to corresponding simulations in LS-DYNA. The two cases that were used in the verification process were the Single Element Test and the Bi-Metal Strip Test. This section will describe the models and the different load cases used in the simulations, as well as the reasons to why these specific models were chosen.

The material properties used for the adhesives in all test cases were for the single component epoxy hybrid adhesive of interest at Volvo Cars. Due to confidentiality material parameters are not included in this report.

Since the purpose of the test cases was to verify the Abaqus implementation against the LS-DYNA implementation, the difference between the results had to be quantified. The quantitative measurement was chosen as the relative error where the results from LS-DYNA were used as the reference. Since the main points of interest were the residual displacement and the residual stress, the notation that will be used for the relative error for the displacement and stress are

$$\delta u = \left| \frac{u_{\text{Abaqus}} - u_{\text{LS-DYNA}}}{u_{\text{LS-DYNA}}} \right|, \tag{4.1}$$

$$\delta \sigma = \left| \frac{\sigma_{\text{Abaqus}} - \sigma_{\text{LS-DYNA}}}{\sigma_{\text{LS-DYNA}}} \right|. \tag{4.2}$$

4.2.1 Single Element Test

The first test case consisted of a single adhesive element with the dimensions 1 x 1 x 1 mm. The single element case was chosen since a model that was as simple as possible was desired. Thereby, the number of potential causes of errors was kept as low as possible, for example in the modelling stage.

The element was chosen to be a first-order hexahedron element and thus had eight nodes, one in each corner. The element with node numbering is shown in Figure 4.4. In Abaqus element formulation "C3D8" was used, and in LS-DYNA element formulation "2" was used.

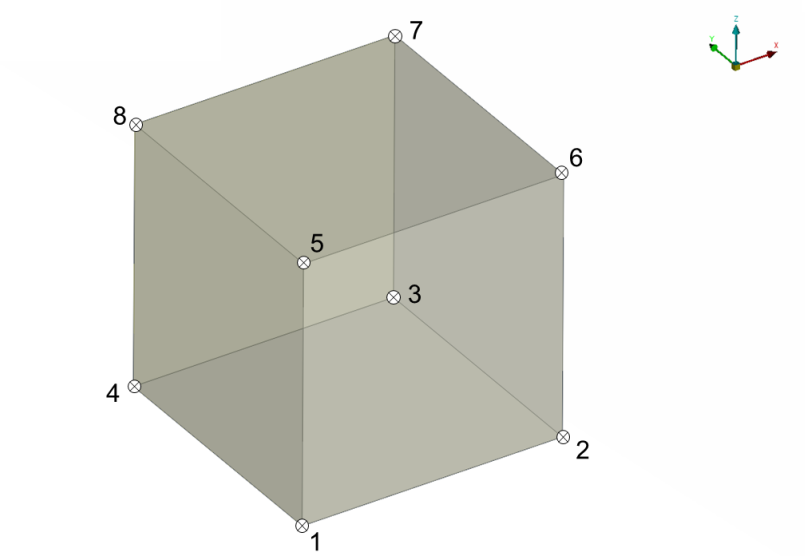

Figure 4.4: Single element model with node numbers.

Three load cases were used to assess the material model implementation in Abaqus, with 1 s as maximum time increment. Details of the load cases are given in the following sections.

4.2.1.1 Load Case I

The first load case consisted of only a thermal load under constrained deformation. The thermal load was defined as a time-varying temperature, applied to each of the eight nodes. The intention of this case was to test that the material response under thermal load was correct, and to induce stresses in the z-direction. The magnitude of the thermal load was varied for the duration of the simulation according to the load curve in Figure 4.5. The duration of the simulation was set to 2400 seconds. The thermal load included two separate heating and cooling phases, with a start and end temperature of 20 °C and a peak temperature of 190 °C.

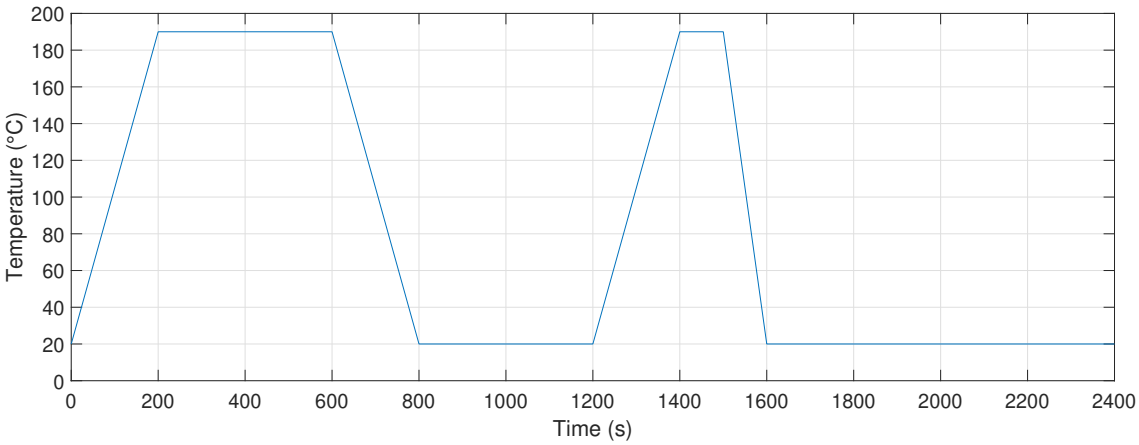

Figure 4.5: Temperature curve for the single element, case I.

Furthermore, all of the nodes were constrained in the z-direction, simulating the situation that the element is restrained between two rigid surfaces. Moreover, to avoid rigid body movement, node #1 was also constrained in the x- and y-direction, and node #2 was also constrained in the y-direction.

4.2.1.2 Load Case II

The second load case consisted of the same thermal load as the first load case. However an additional mechanical load was applied in form of a 0.5% tensile strain in the z-direction. The strain was applied linearly between the times 950 s and 1050 s, as can be seen in Figure 4.6. Furthermore, the strain was applied as increasing displacement of the four nodes on top of the element. The remaining nodes were constrained in the same way as in case I.

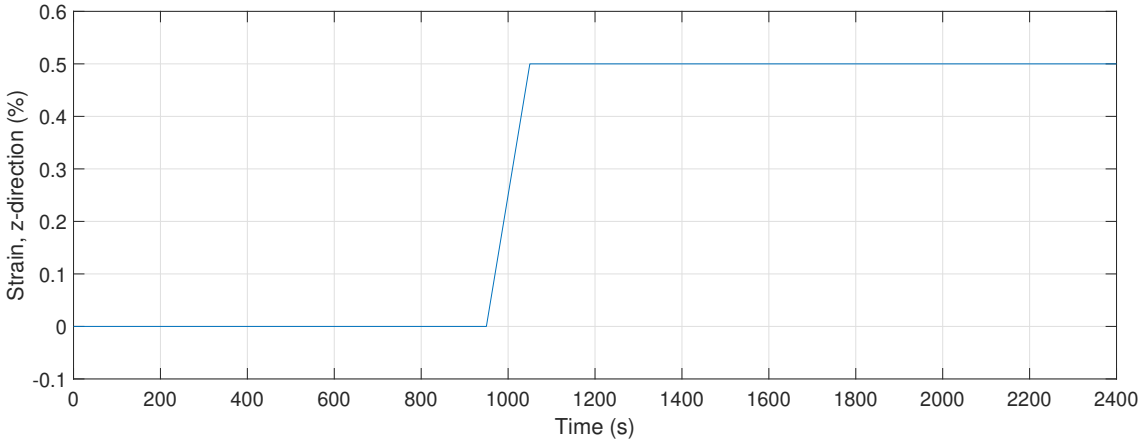

Figure 4.6: Strain curve for single element, case II.

4.2.1.3 Load Case III

The third load case consisted of the same loads as in case II, with the addition of a shear strain 0.5% in the zx-direction. Thereby the single element was subjected to both a tension strain and a shear strain simultaneously. Both the strain in tension and in shear were applied according to Figure 4.6, and both strains were applied on the four topmost nodes. This load case was chosen to induce a multi-directional stress state in the element, while still keeping the model as simple as possible.

4.2.2 Bi-Metal Strip Test

The second test was performed on a Bi-Metal Strip. As the name suggests, the model consisted of two metal strips, which were described as joined together with the adhesive. One strip was given the material properties representative for DP600 steel and the other for Al6060 T6 aluminium.

The two strips were geometrically identical with the dimensions 100 x 20 x 2 mm. The simulation model can be seen in Figure 4.7, where red represents steel and blue represents aluminum. The adhesive layer between them had a thickness of 0.3 mm, and in Figure 4.7 it is shown in yellow. Moreover, perfect adhesive coverage for the region between the steel and aluminium strips was assumed. The maximum time increment size used for the Bi-Metal strip was 1 s.

The model was meshed with hexahedron elements. The model contained four elements in the thickness for each respective part, thus resulting in the element sizes 1 x 1 x 0.5 mm in the metal strips and 1 x 1 x 0.075 mm in the adhesive.

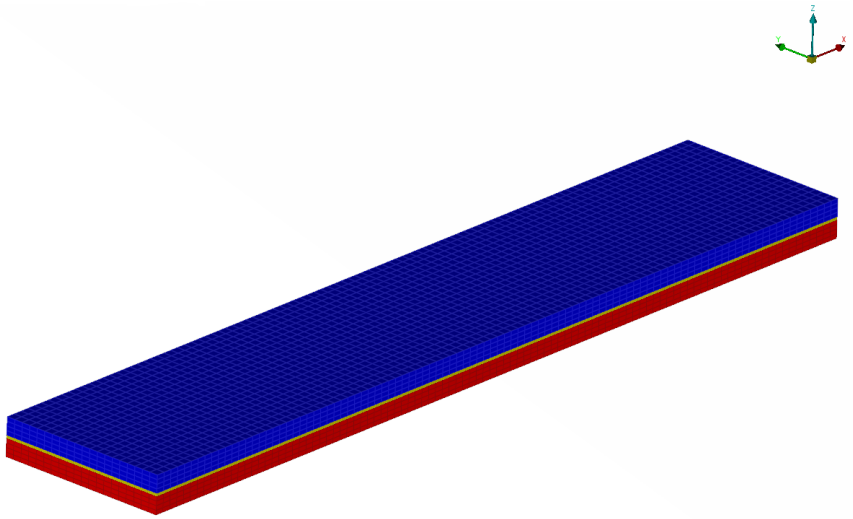

Figure 4.7: Model of the Bi-Metal Strip

As in the Single Element case, element formulation "C3D8" was used in Abaqus and element formulation "2" was used in LS-DYNA for all elements. The connections between the adhesive elements and the elements on the metal strips were realized by shared nodes.

One of the short sides of the Bi-Metal Strip was constrained in the x-direction, and one of the long sides was constrained in the y-direction. Furthermore, one of the corner nodes was constrained in all translational directions to prevent rigid body motion. The boundary conditions are also illustrated in Figure 4.8.

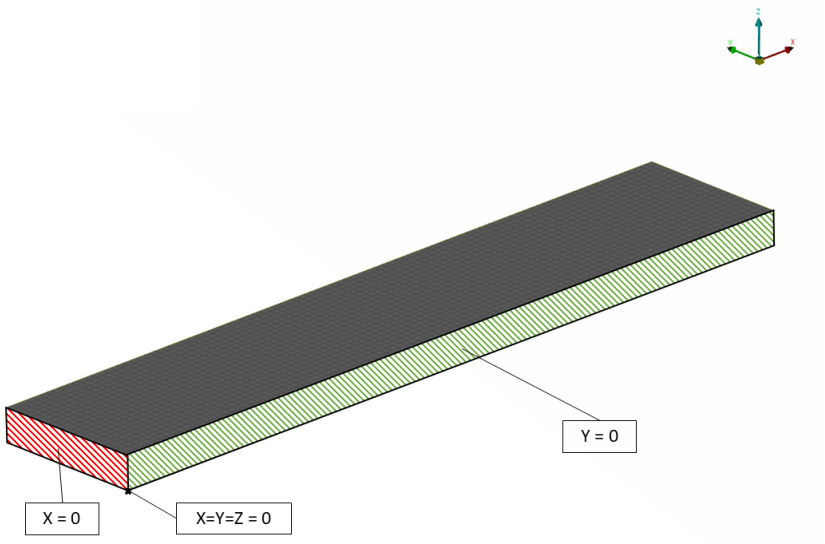

Figure 4.8: Boundary conditions for the Bi-Metal Strip.

In this test, a varying thermal load was applied on all nodes homogeneously. The

temperature applied corresponded to a curing oven, the curve for the temperature can be seen in Figure 4.9.

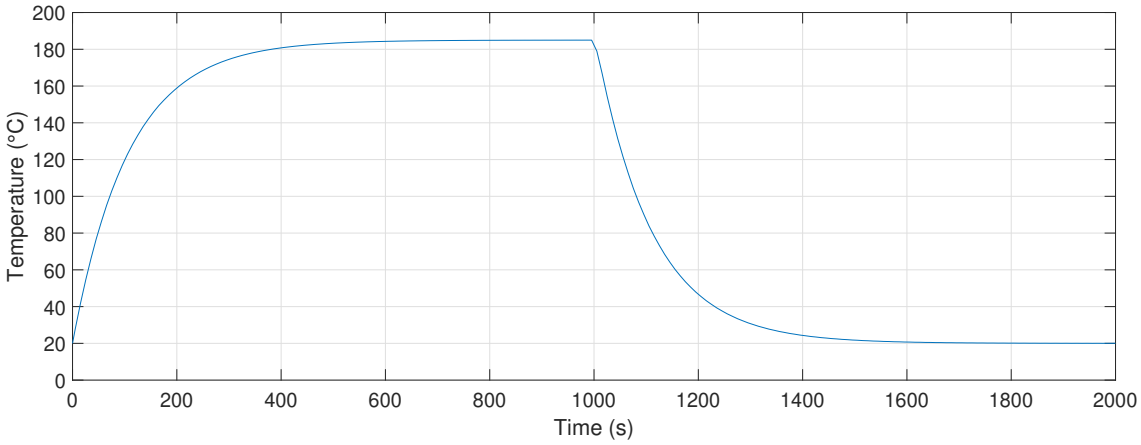

Figure 4.9: Temperature curve for the Bi-Metal Strip.

4.2.3 Convergence Study

As some inconsistencies were noted in the results from the Bi-Metal Strip, even between different runs in the same software, it was determined that a time step convergence study was to be conducted. The purpose of the convergence study was to investigate if the time increment size had an influence on the results for the adhesive. The convergence study was conducted in both Abaqus and LS-DYNA. It was performed by simulating the Bi-Metal Strip as described in Section 4.2.2 with different values for the maximum increment size. The maximum increment sizes that were evaluated were 30, 10, 1, 0.5, and 0.25 s. The convergence study was conducted with the automatic incrementation enabled in both software, meaning that the solver will automatically reduce the size of the time increment after a number of iterations where a solution could not be found, thereby increasing the chances that the solver will find a converged solution.

4.3 Comparison With Physical Test

The material model implementation was also used in a third case, the Hat Profile, in this case there was no comparison between Abaqus and LS-DYNA, only between Abaqus and test results from a physical test that had previously been performed.

4.3.1 Hat Profile

The Hat Profile component consisted of a DP600 steel “hat” and an Al6060 T6 aluminium “lid”. The model of the Hat Profile component can be seen in Figure 4.10, where the lid is shown in blue and the hat is shown in red.

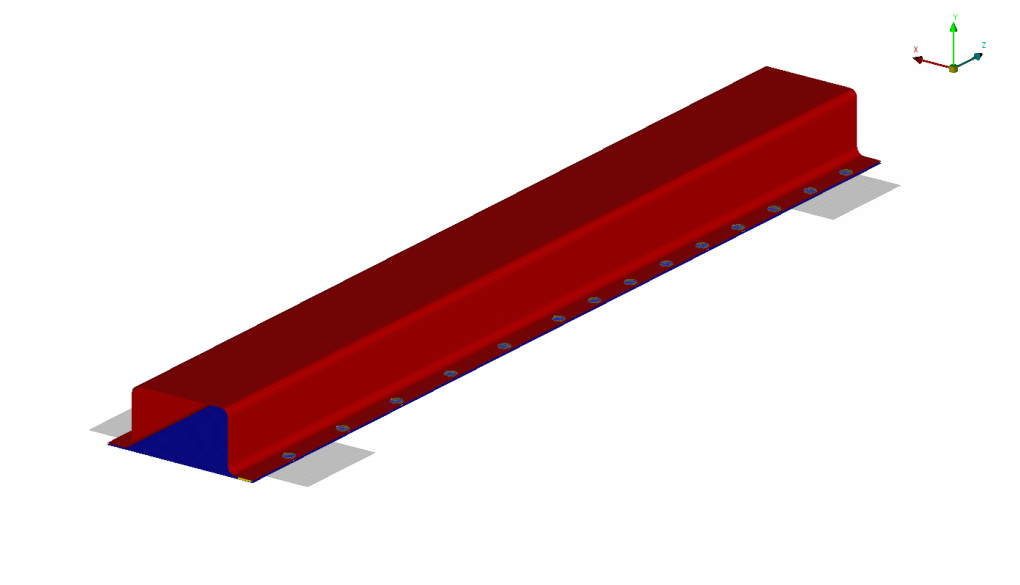

Figure 4.10: Model of the Hat Profile component.

The Hat Profile had a length of 700 mm and a width of 116 mm. The thickness of the hat was 1.5 mm and the thickness of the lid was 0.95 mm. The adhesive layer between them had a thickness of 0.3 mm. The additional dimensions of the Hat Profile can be seen in Figure 4.11.

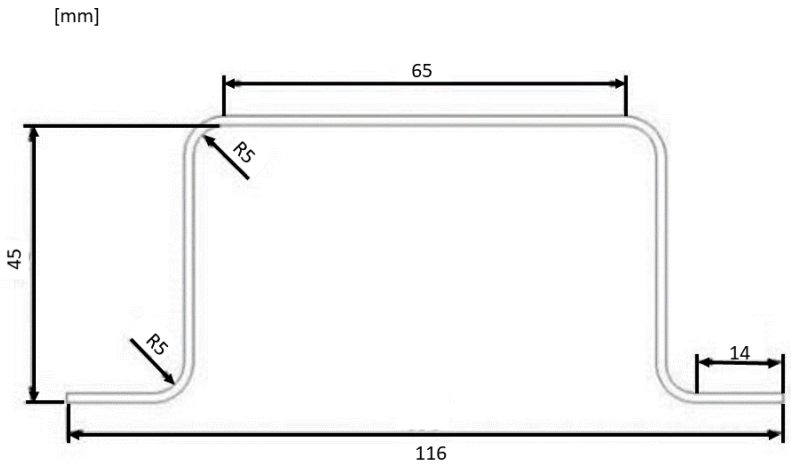

Figure 4.11: Dimensions of the hat in the Hat Profile component.

The physical test of the Hat Profile was carried out in the MULTIM project, which was a predecessor to the MADBOND project. The Hat Profile used in the test was joined together with EJOWELD® CFF joints on both flanges. This joint can be

seen as a mix of a weld and a rivet, as the joint gets attached to the steel through friction welding and to the aluminium as a traditional rivet. Adhesive was applied to one of the flanges. Two different pitches were used for the rivets, which is the distance between two adjacent rivets, a 60 mm pitch was used for half the length of the component and a 40 mm pitch was used for the other half of the length, illustrated in figure 4.12.

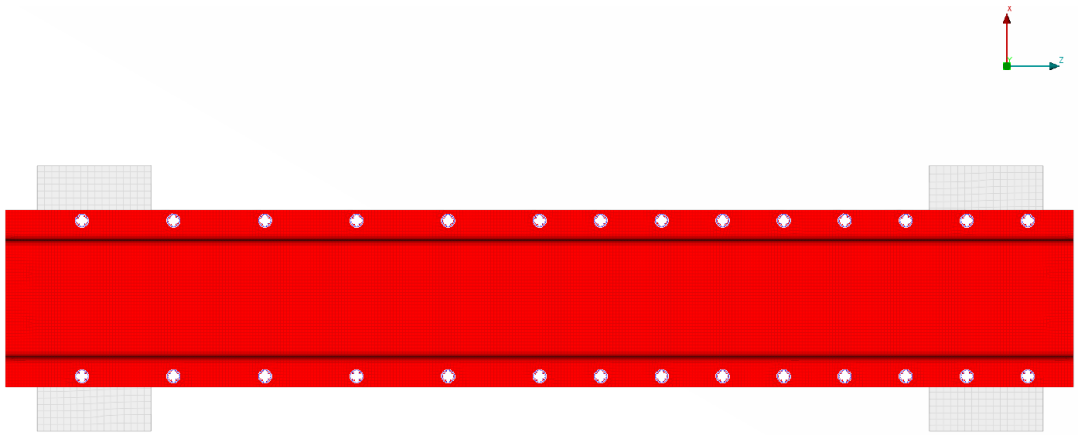

Figure 4.12: View from above on the Hat Profile, showing the fasteners in white.

The Hat Profile was set into an oven, where it was subjected to varying temperatures for 2000 seconds. The temperature profile that was used in the oven can be seen in Figure 4.13. The component was furthermore scanned with a 3D-scanning device before, during, and after being in the oven, to accurately capture the deformations of the component.

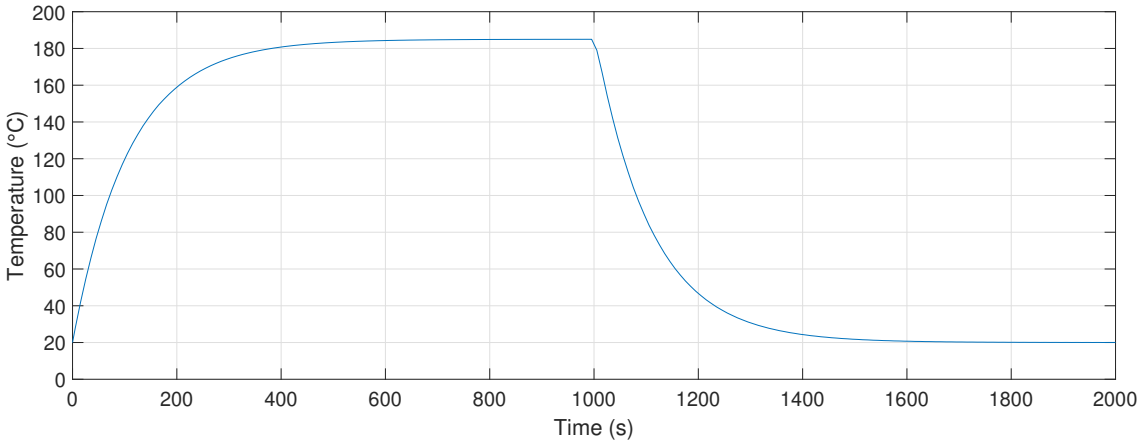

Figure 4.13: Temperature curve for the Hat Profile.

In the simulation model of the Hat Profile, the hat, lid, and supports were meshed with shell elements with the element formulation “S4”, with an element size of 2 x 2 mm. The adhesive was meshed as a solid mesh with the element size 7 x 5 x 1.125 mm

and the element formulation “C3D8”. The rivets were realized with SPIDER2 FE-representation, which connected the two parts meshed with shell meshes with a beam element. This FE-representation is furthermore illustrated in Figure 4.14a. The metal-adhesive-metal interaction on one of the flanges had the FE-representation RBE3-HEXA-RBE3, which connected the solid meshed adhesive to the mid-plane of the two with shell meshes. The RBE3-HEXA-RBE3 FE-representation is illustrated in Figure 4.14b.

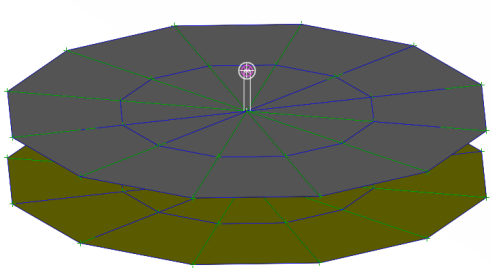

(a) Rivet represented with SPIDER2.

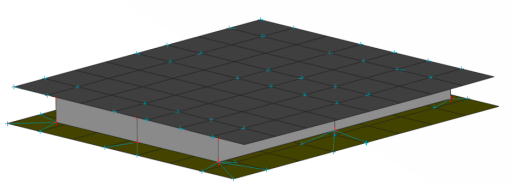

(b) Adhesive represented with RBE3-HEXA-RBE3.

Figure 4.14: FE-representations of connections.

The temperature load in the simulation model used the same temperature curve as in the physical test, seen in Figure 4.13. In the simulation this temperature was applied to all nodes, with the exception of the two supports.

One aspect that should be noted from the test results is that there was evidence of failure in the adhesive at the locations of the largest residual deformations. This is of significance since the aspect of adhesive failure is not included in the simulation model. It should also be mentioned that there were some differences in the setup of the component in the test and in the simulation. In the simulation, the component was laying down, supported by two rigid supports, whilst it in the test setup was positioned upright.

There could also have been other aspects in the test that had an affect on the results, which were not included in the simulation. Such aspects could have been the application of the adhesive, and that perfect coverage was not achieved, or initial deformation in the test component due to the process of applying the rivets. These aspects therefore has to be taken into consideration when comparing the results from the simulations with the test results.

5

Results & Discussion

In this chapter the results from the cases presented in the method chapter are presented. This includes comparisons between Abaqus and LS-DYNA for the Single Element and the Bi-Metal Strip simulations, and the comparison between Abaqus and the physical test for the Hat Profile component.

5.1 Verification of Abaqus Implementation

The results from the verification tests of the three single element load cases and the Bi-metal strip test will be presented for both LS-DYNA and Abaqus in the following section.

5.1.1 Single element

In this section the results from the simulations of the three single element load cases will be presented. The results for the stresses are calculated as the mean of the 8 integration points of the element, and the results for the displacements are presented for node # 7, as defined in Figure 4.4.

5.1.1.1 Load Case I

The degree of cure (DoC) for the single element can be seen in Figure 5.1. From these results, it can be seen that LS-DYNA and Abaqus gave the same results except for the first increment in the simulation, which can be seen in the enhanced part of Figure 5.1. LS-DYNA starts with a DoC equal to 0.01, whilst Abaqus has a value of zero at that point. This was also the case for the other solution-dependent state variables.

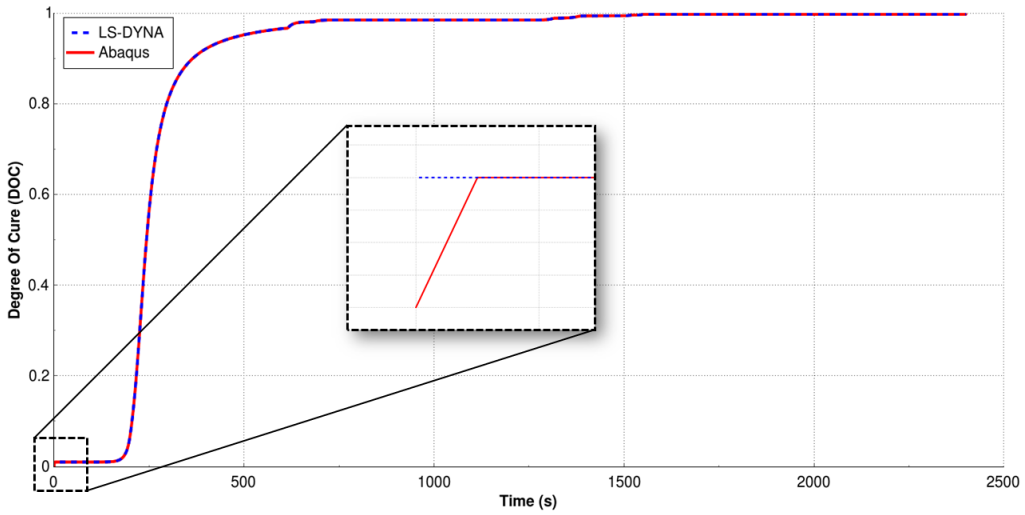

Figure 5.1: Degree of Cure, load case I.

The difference in the first increment seen in Figure 5.1 can however be explained by how Abaqus and LS-DYNA output results for solution-dependant state variables in the first increment. The solution-dependent state variables are initialized within the umat42 subroutine obtained from RISE. In LS-DYNA, the initialized values from the subroutine are written to the result file. In Abaqus on the other hand, the initialized values are not written to the result file, the first results are written at the end of the first increment.

Solution-dependent state variables can however be initialized in a user subroutine called "SDVINI" in Abaqus. With that said, the solution-dependent state variables are already initialized in the RISE subroutine, which means that initialization performed in the SDVINI subroutine would not have any influence on the calculations, only on the output results at time $t = 0$.

Furthermore, the solution-dependent state variables are not of any particular interest at Volvo Cars, as it is mainly the stresses and displacements that are of interest. Therefore it was opted not to use the user subroutine SDVINI at this stage.

The Von Mises stress for the Single Element can be seen in Figure 5.2. The difference in magnitude between the two software is small for the duration of the simulation. With a relative error $\delta\sigma = 0.3\%$ for the the residual stress in Abaqus compared to LS-DYNA. The total nodal displacement seen in Figure 5.3, exhibited a larger difference, especially when the maximum displacement is reached. The residual displacement had a relative error $\delta u = 1.7\%$, which is still well below the allowable limit.

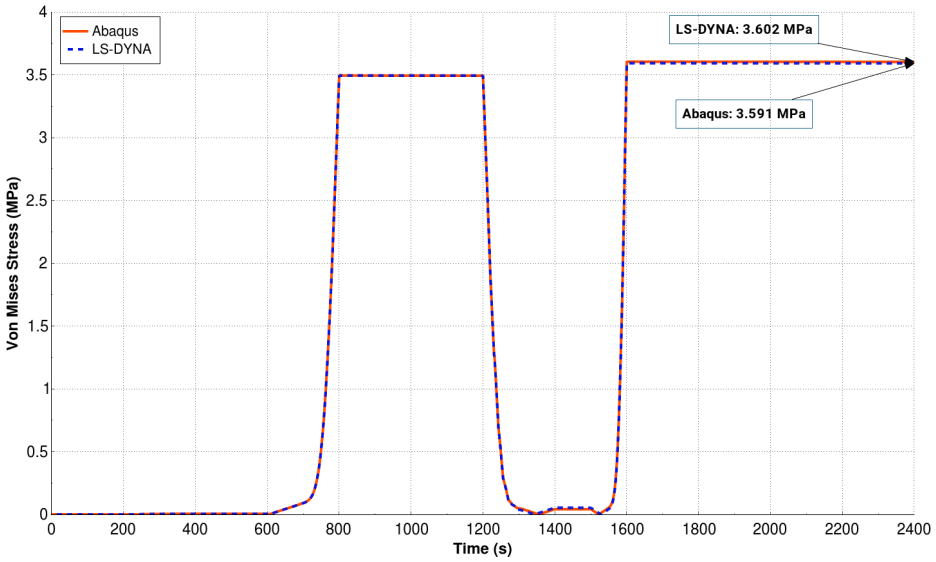

Figure 5.2: Von Mises Stress for single element, load case I

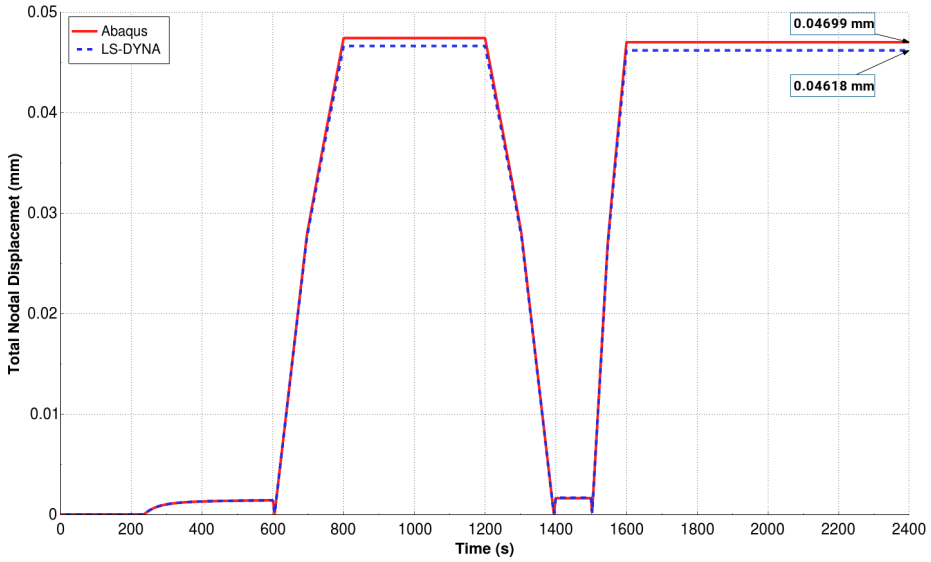

Figure 5.3: Total nodal displacement for node #7, load case I.

Even though some differences between Abaqus and LS-DYNA were noted in the results for the stress and displacement, they were all within the defined tolerances of 10 %, and therefore they were not investigated further.

5.1.1.2 Load Case II

The Von Mises stress for Load Case II can be seen in Figure 5.4. The maximum stress was approximately 7.6 MPa when the strain was applied. The results showed minor differences between LS-DYNA and Abaqus, with a relative error $\delta\sigma = 0.3\%$ for the residual Von Mises stress. The resulting displacement seen in Figure 5.5,

had slightly lower magnitude in LS-DYNA compared to Abaqus, most notably at the times 800 s to 1200 s, and 1600 s to 2400 s. The residual displacement resulted in the relative error $\delta u = 1.75\%$.

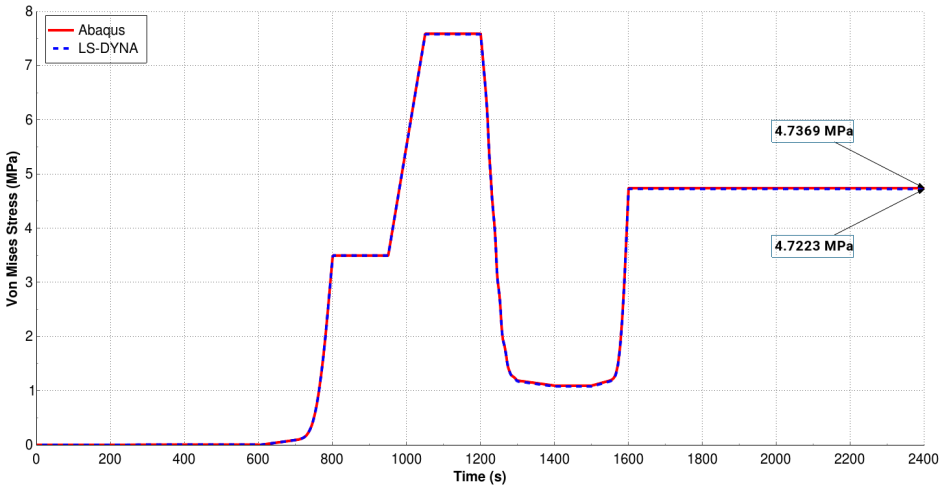

Figure 5.4: Von Mises Stress for single element, load case II

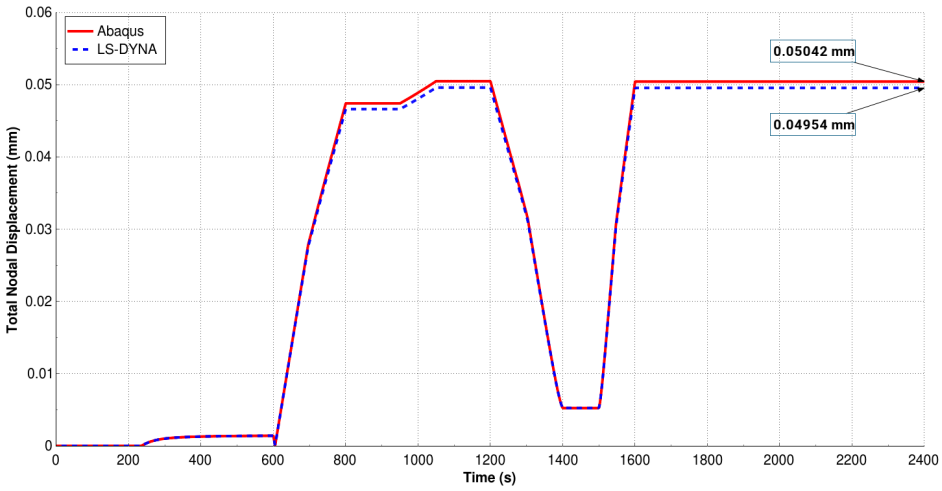

Figure 5.5: Total nodal displacement for node #7, load case II.

The results for Load Case II indicated that the material model implementation in Abaqus gave accurate results in an uni-directional load scenario, with relative errors for both the stress and displacement that was within the defined limits.

5.1.1.3 Load Case III

The Von Mises stress, seen in Figure 5.6, gave the same shape as the stress in Load Case II, but with larger magnitude. The results from Abaqus and LS-DYNA matched well also in this case, as the residual Von Mises stress had the relative error $\delta\sigma = 0.17\%$. The displacement, seen in Figure 5.7, gave a similar shape as in

load case II, although with a slightly smaller magnitude. The relative error of the displacement in load case III was $\delta u = 0.13\%$.

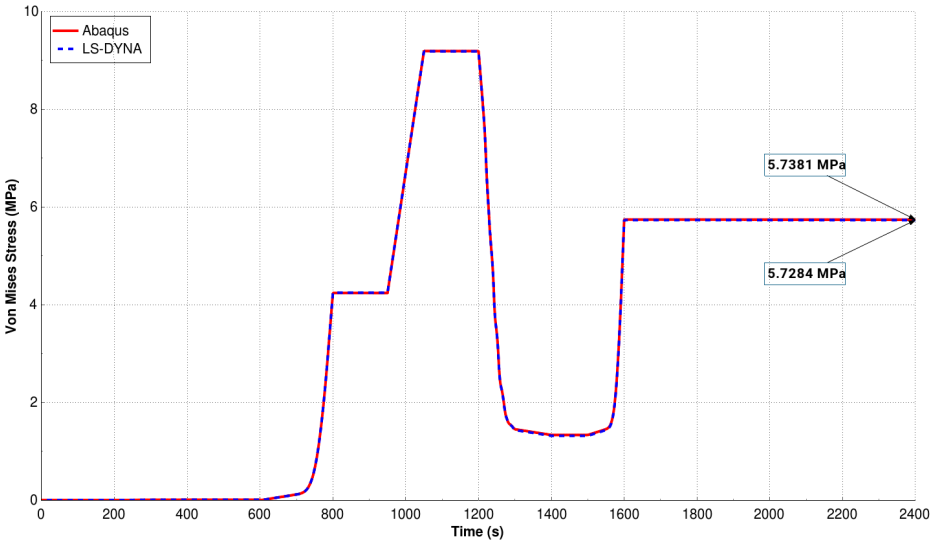

Figure 5.6: Von Mises Stress for Single Element, load case III

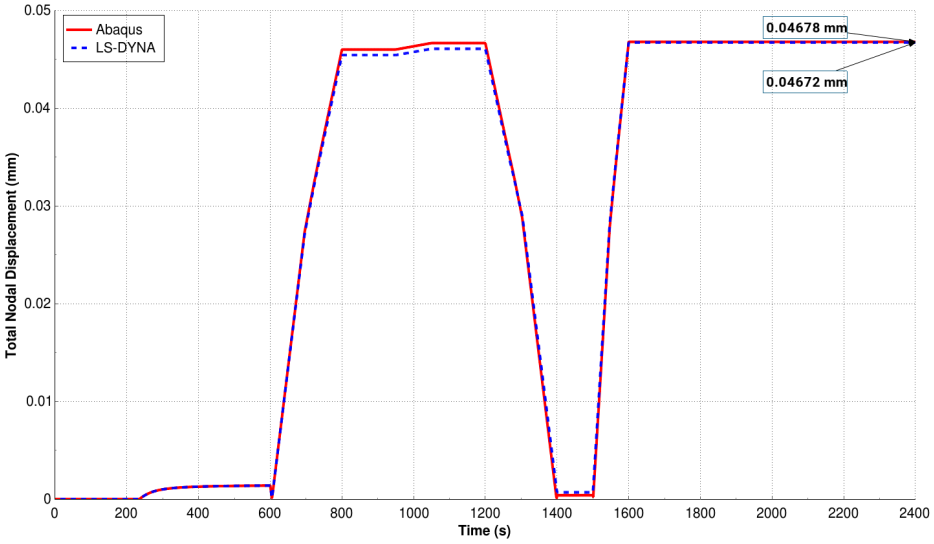

Figure 5.7: Total nodal displacement for node #7, load case III.

Although there were some minor differences in the results between the two solvers, as the relative error was within the defined limits for both the residual stress and residual displacement in all load cases, the Abaqus implementation was deemed to have been successfully verified for the single element case. These results indicated that the Abaqus implementation captured the correct material behavior both in uni-directional and multi-directional loading conditions.

5.1.2 Bi-Metal Strip

The results for the stress are presented for two elements on the Bi-Metal Strip, #21835 (edge), and #24832 (middle), seen in Figure 5.8. These two elements were positioned in the middle of the thickness of the adhesive. For simplicity element #21835 will be referred to as the "edge element" and #24832 as the "middle element". The results for the displacement are furthermore presented for node #120724, located on the edge element, and node #17135, located on the middle element.

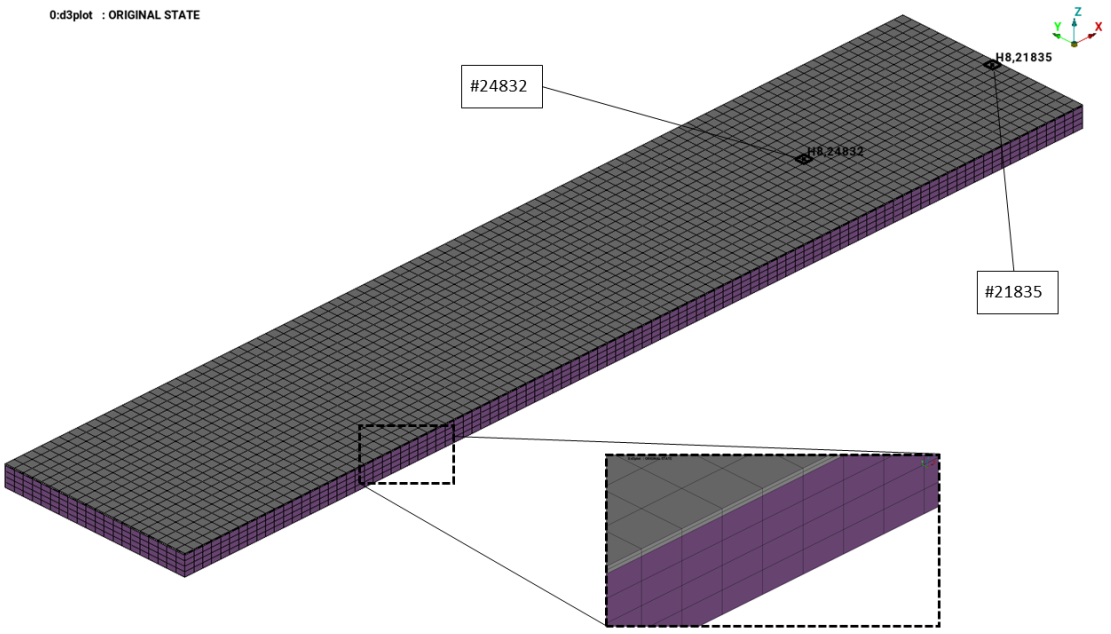

Figure 5.8: Element positions in the Bi-Metal Strip with steel (purple) and half of the adhesive layer (grey).

The Von Mises stresses in the edge and middle element are shown in Figure 5.9, with a zoom of the response at $t = 2000$ s in Figure 5.10. The results from LS-DYNA and Abaqus are similar for both the middle and the edge element throughout the duration of the simulation. The relative error for the residual stress was $\delta\sigma = 1.02\%$ for the middle element and $\delta\sigma = 1.69$ % for the edge element.

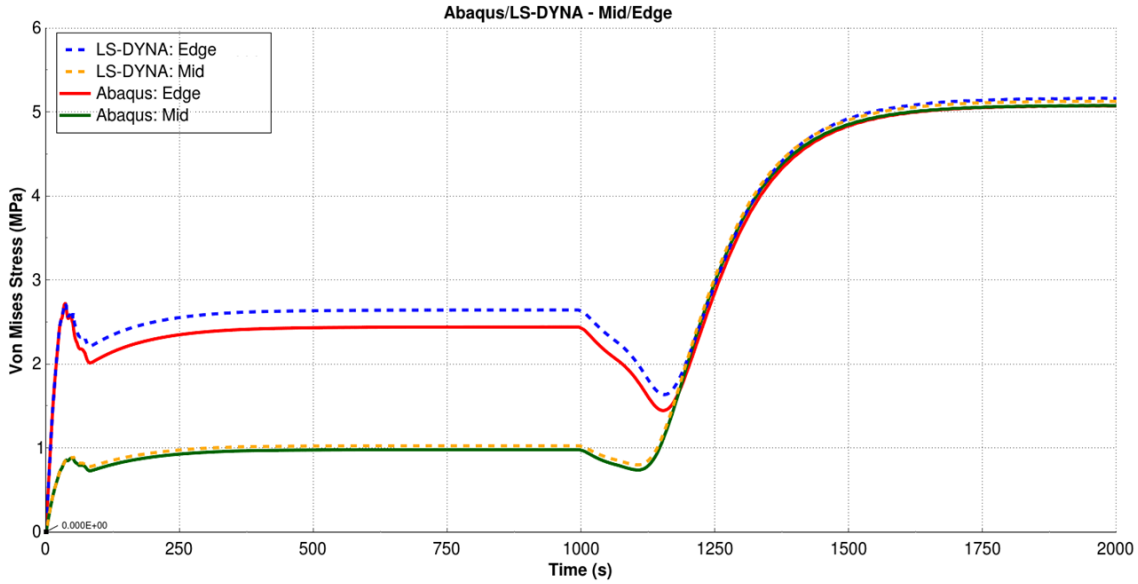

Figure 5.9: Von Mises stress in elements #21835 & #24832.

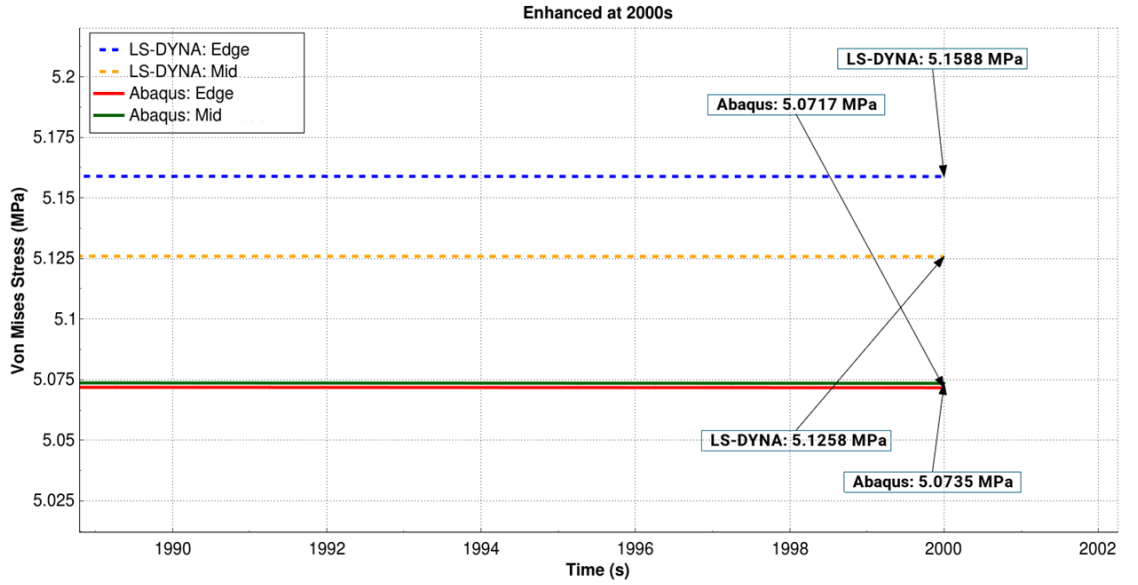

Figure 5.10: Residual Von Mises stress in elements #21835 & #24832 at t=2000s.

The nodal maximum displacement in the z-direction reached approximately 1.3 mm and 0.9 mm for the edge and middle element, respectively, at the peak temperature ($t = 1000$ s), which can be seen in Figure 5.11. The residual displacement can be seen in Figure 5.12, showing Figure 5.11 zoomed in at the last 150 s of the simulation. The relative errors were $\delta u = 6.72\%$ and $\delta u = 6.80\%$ for the edge and middle element respectively.

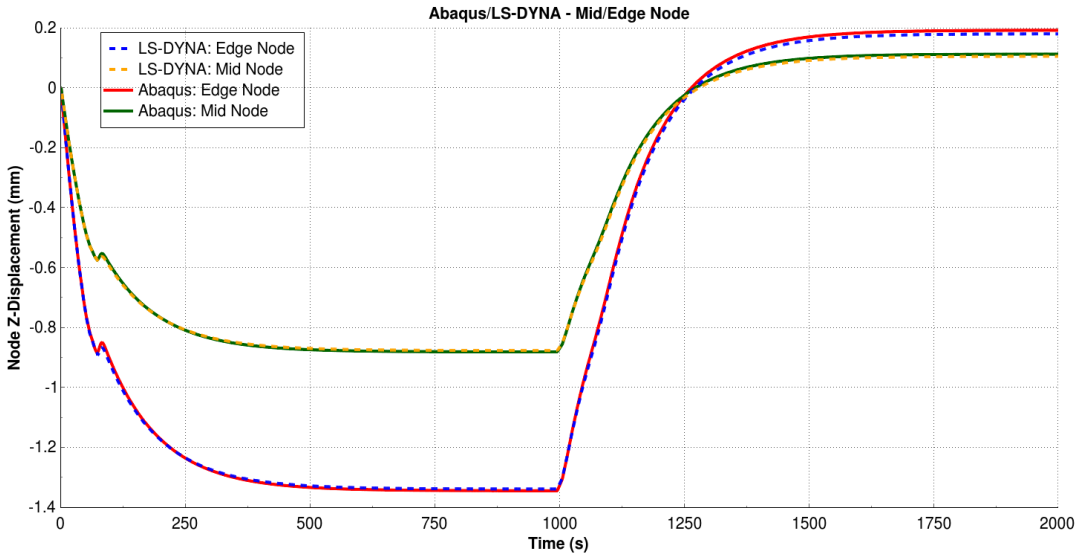

Figure 5.11: Nodal z-displacement for nodes #120724 & #17135.

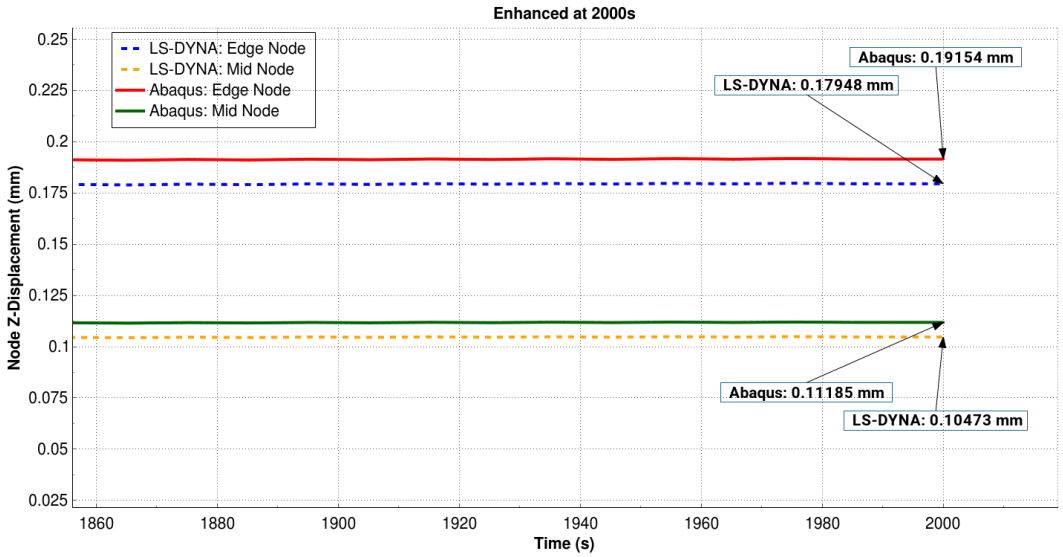

Figure 5.12: Nodal z-displacement for nodes #120724 & #17135, zoomed at last 150 s.

In the cooling phase ($t > 1000$ s), the magnitude of displacement decreases, as can be seen in Figure 5.11. Due to the small magnitudes, small variations between LS-DYNA and Abaqus can result in a large relative error. From the results however the relative error was still below the 10% limit, thus indicating that the relative error between LS-DYNA and Abaqus is minor even for small magnitudes.

The residual Von Mises stress on the short side facing the negative x-direction is also shown in a contour plot in Figure 5.13. The results are close to identical, with only minor differences in magnitudes on a few elements.

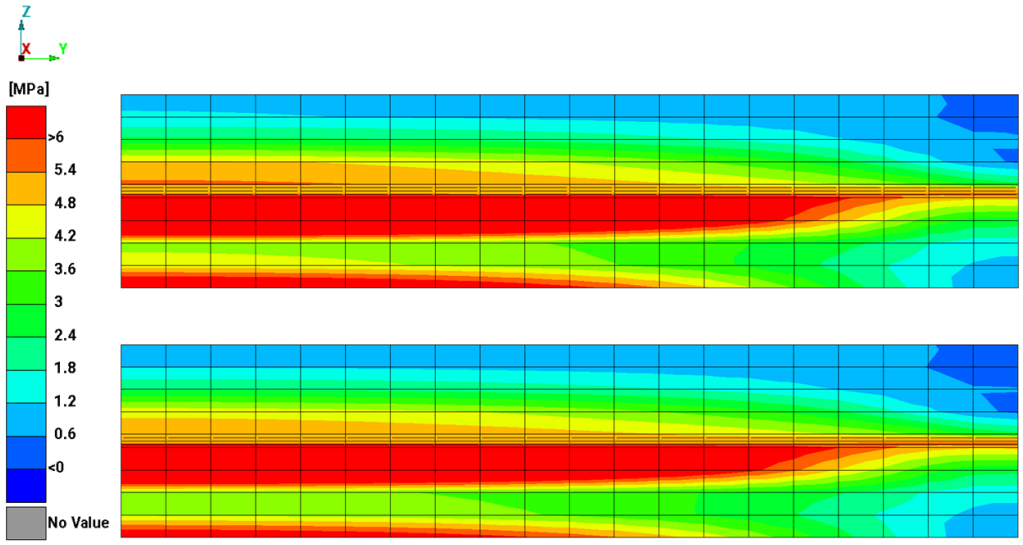

Figure 5.13: Residual Von Mises stress on the right short side of the Bi-Metal Strip, Top: Abaqus, Bottom: LS-DYNA.

The distribution of the Von Mises stress on the bottom of the adhesive layer at $t = 1000$ s can be seen in Figure 5.14. From these results it was noted that both the stress distribution and the stress magnitude match well between the two software.

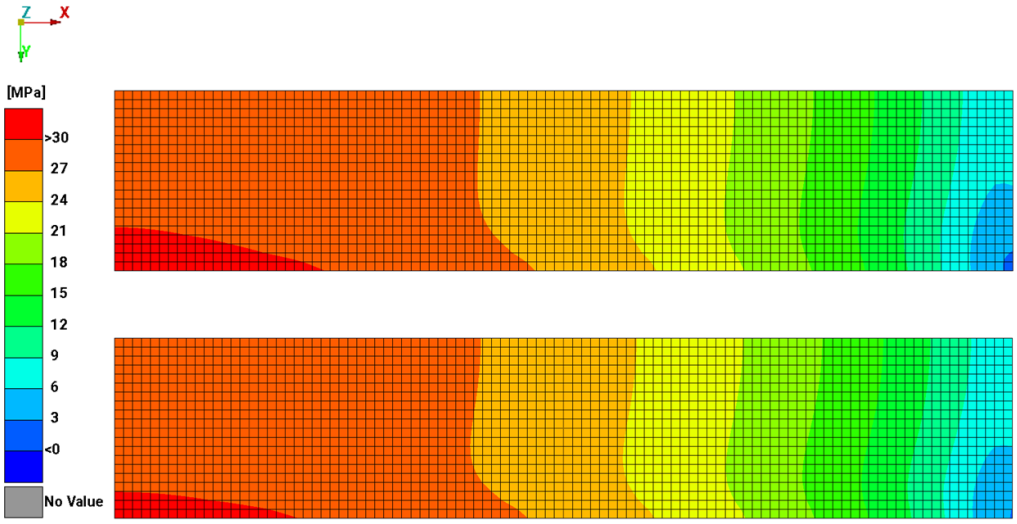

Figure 5.14: Von Mises stress on the underside of the adhesive in the Bi-Metal Strip at t=1000 s, Top: Abaqus, Bottom: LS-DYNA.

The displacement in the z-direction of the Bi-Metal Strip at time t=1000 s is shown in Figure 5.15. The displacement in the z-direction, obtained at the bottom side of the adhesive layer at the same time can be seen in Figure 5.16.

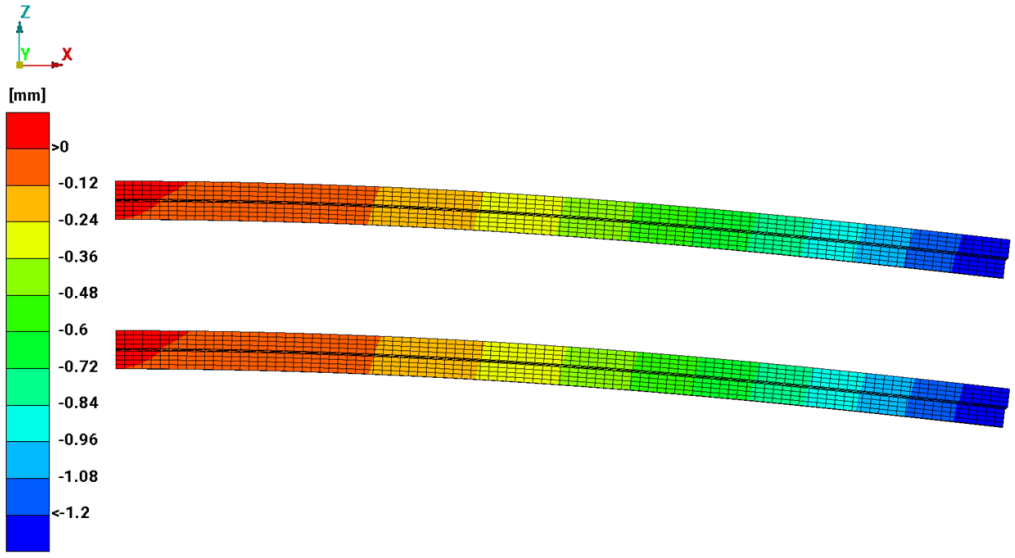

Figure 5.15: Z-displacement distribution on the side of the Bi-Metal Strip at $t = 1000$ s. Scale factor: 5, Top: Abaqus, Bottom: LS-DYNA.

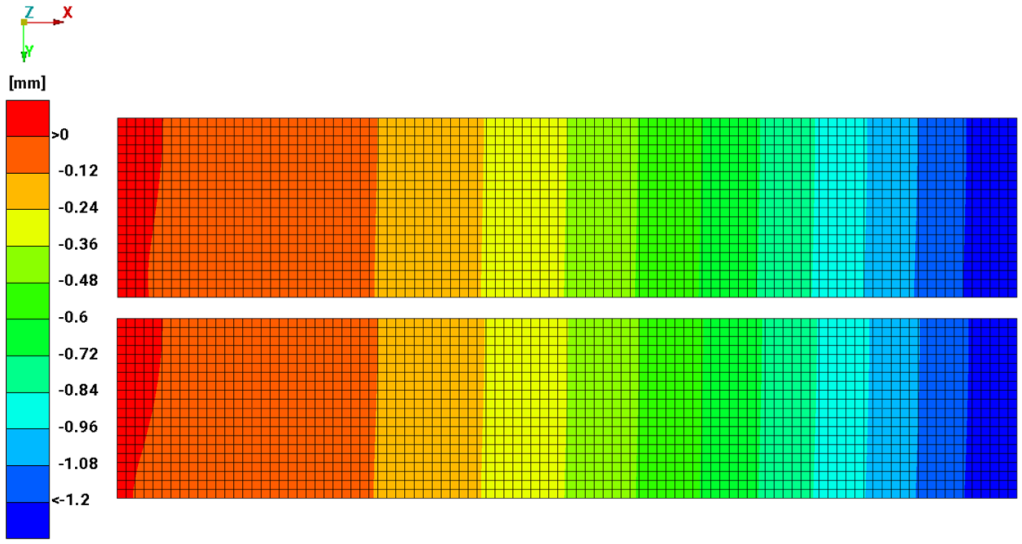

Figure 5.16: Z-displacement distribution on the bottom side of the Bi-Metal Strip at $t = 1000$ s, Top: Abaqus, Bottom: LS-DYNA.

From the contour plots, the displacement and Von Mises stress correlation well between LS-DYNA and Abaqus, indicating that the Abaqus implementation captures the same behavior as in LS-DYNA over all elements throughout the simulations of the Bi-Metal Strip.

When performing the simulations of the Bi-Metal Strip, one issue with the material model implementation in Abaqus was noted. This issue was that it was not possible

to use the material model when performing the simulation using parallel processing with MPI (Message Passing Interface) or threads. A workaround for this issue was used through the option threads=1 when creating the job in Abaqus. This option means that each core used for calculations is working on a separate thread with separate tasks, as opposed to several cores splitting the work of a task.

The reason that this issue was not noticed earlier was that in the Single Element case, only one core was used for the calculations, as is it not possible to split the workload of a single element over several cores.

As a result of this issue, all the following simulations were performed with the options threads=1 and cpus=16 in Abaqus, meaning that the simulations were performed on 16 cores, with each core having its own thread.

5.1.3 Convergence Study

When initially investigating the difference in magnitude of the stress and displacement in LS-DYNA and Abaqus, the time increment was maximizes to 10 s. It was noted that there were some differences in the magnitudes, and it was also noted that the difference originated in a region where the automatic incrementation in Abaqus reduced the increment size. In LS-DYNA on the other hand, there were no reduction of the time increment size, which can be seen in Figure 5.17. With this result as basis, a convergence study for the time increment size was conducted.

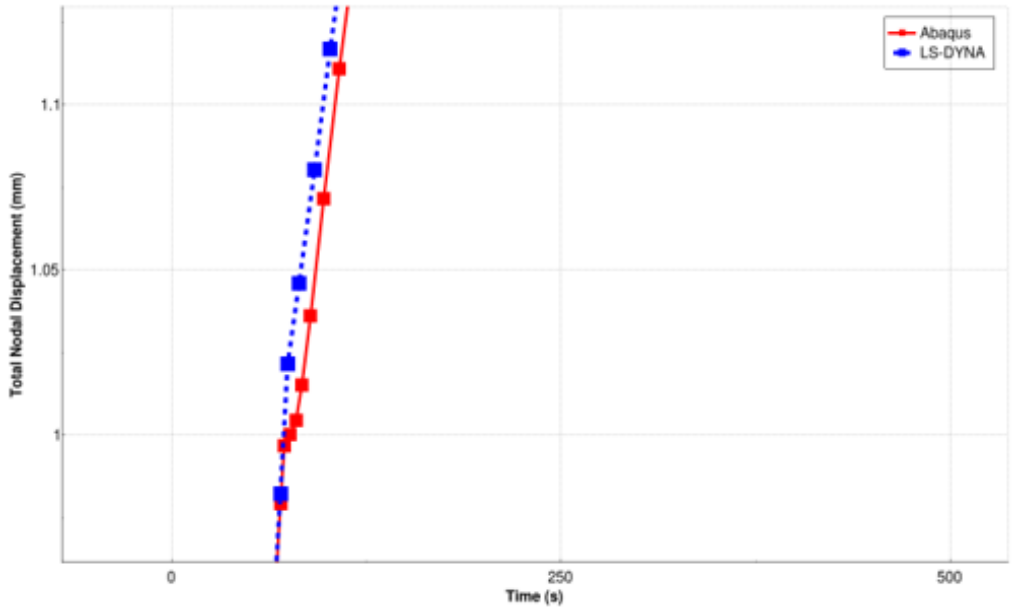

Figure 5.17: Zoom of total nodal displacement with time steps shown at critical region. Maximum increment size 10 s.

In the convergence study, the incrementation influence on the displacement, degree of cure, and stress in Abaqus and LS-DYNA were all investigated.

The increment influence on the nodal z-displacement can be seen in Figures 5.18 and 5.19 for Abaqus and LS-DYNA, respectively.

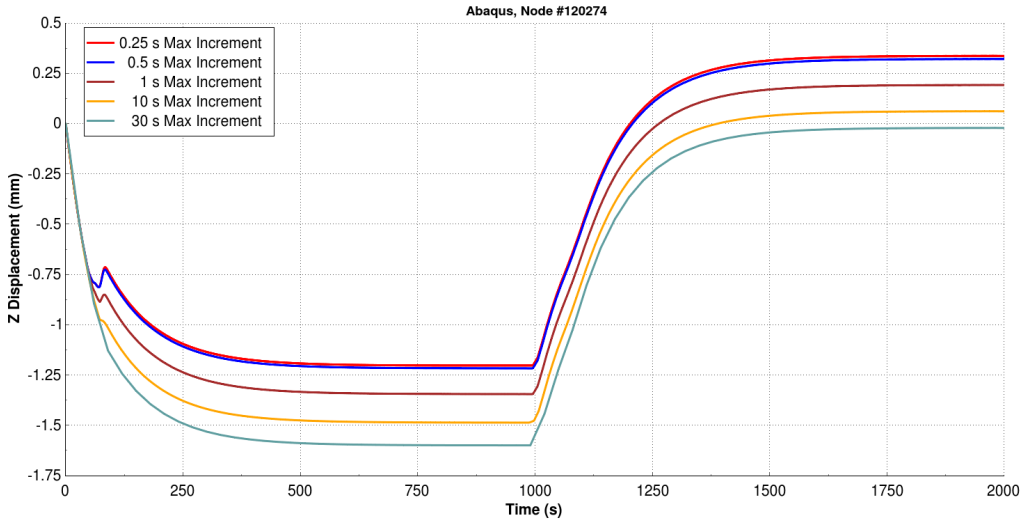

Figure 5.18: Convergence study, Abaqus, total nodal displacement.

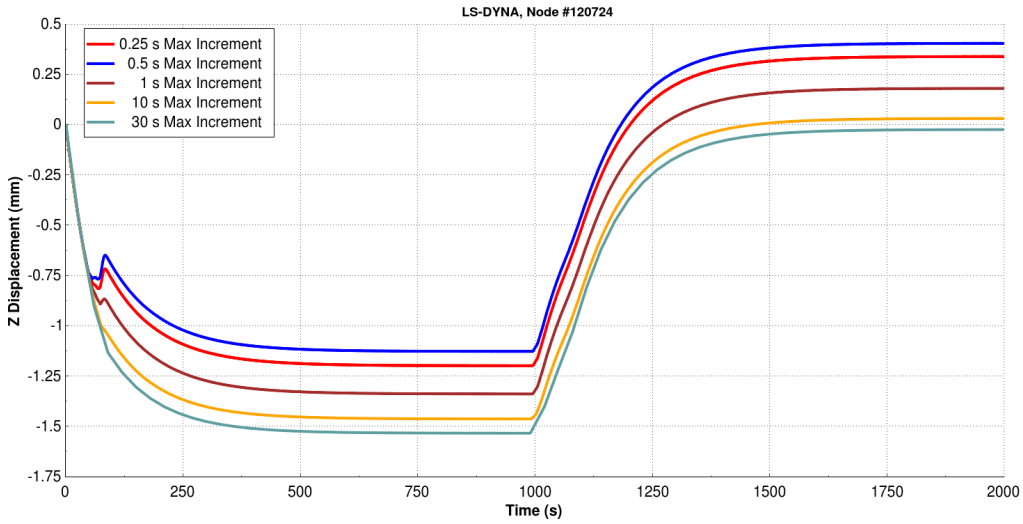

Figure 5.19: Convergence study, LS-DYNA, total nodal displacement.

From the figures, it is clear that the time increment size did show to have a major influence on the results in both Abaqus and LS-DYNA, and it was noted that the differences in both solvers originated from the initial heating phase. After the heating phase, the relative error between the different solutions is almost constant. A smaller increment size resulted in a larger residual displacement, as seen in Figures 5.18 and 5.19. In Abaqus, the solution reached convergence at a maximum time increment size of 0.5 s. There were some inconsistencies in the results from LS-DYNA, as the 0.5 s maximum increment size resulted in a larger residual displacement than the 0.25 s maximum increment size. The reason for this is not entirely clear, but

when inspecting the results, the difference seemed to come from a single increment at time 50.1 s, where the quasi-newton solver had trouble reaching convergence and therefore reformed the stiffness matrix. Considering the general trend that was apparent in both Abaqus and LS-DYNA, it was in the end concluded that the result for 0.5 s maximum increment in LS-DYNA was an outlier.

The results for the degree of cure with different maximum increment sizes in Abaqus and LS-DYNA, can be seen in Figures 5.20 and 5.21, respectively.

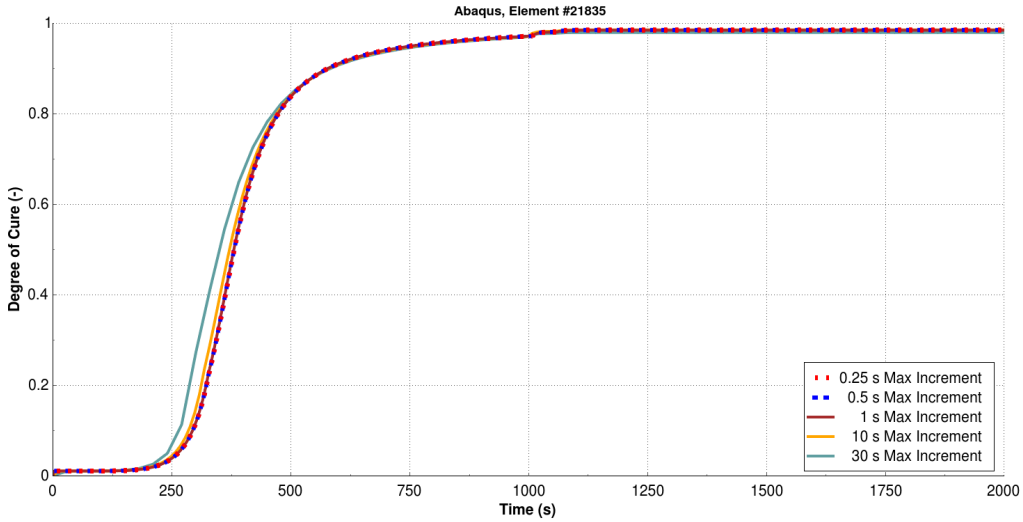

Figure 5.20: Convergence study, Abaqus, degree of cure.

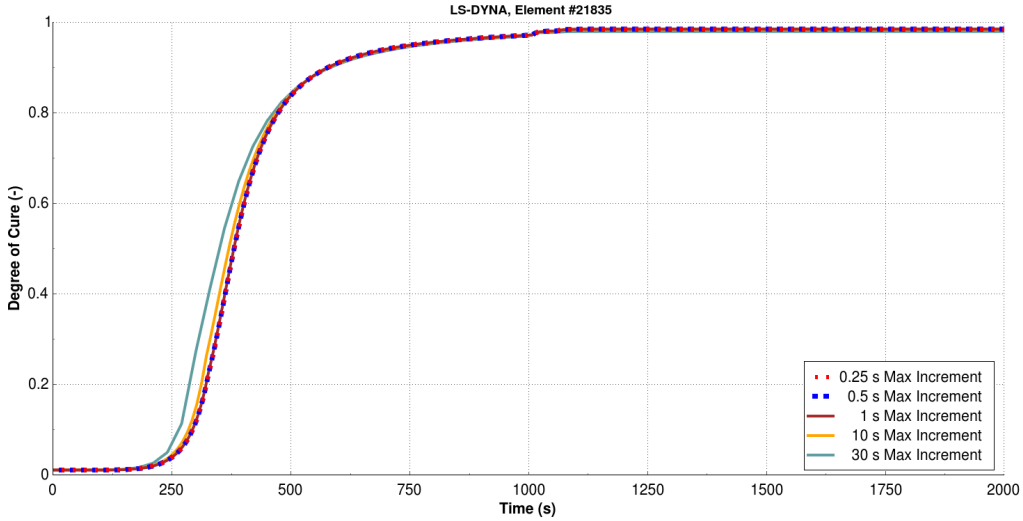

Figure 5.21: Convergence study, LS-DYNA, degree of cure.

Due to the high rate of cure between times $t = 250$ s and $t = 500$ s, small deviations between the time increments resulted in a significant difference in the DoC. This can be exemplified by the LS-DYNA results from the maximum increment sizes 0.25

s and 30 s at time $t = 360$ s. At this instance in time, the predicted degree of cure when using a maximum increment size of 0.25 s is 0.3885, whilst it is 0.544 with a maximum increment size of 30 s. This is especially significant since the gel point of the adhesive is at a degree of cure of 0.42, meaning that one of the solutions was significantly past the gel point as the other had not reached it yet.

After $t \approx 500$ s the results are similar for all time increment sizes in both LS-DYNA and Abaqus, although it should be noted that a smaller maximum increment size resulted in a slightly higher final degree of cure.

The Von Mises stress for different maximum increment sizes can be seen in Figures 5.22 and 5.23 for Abaqus and LS-DYNA respectively.

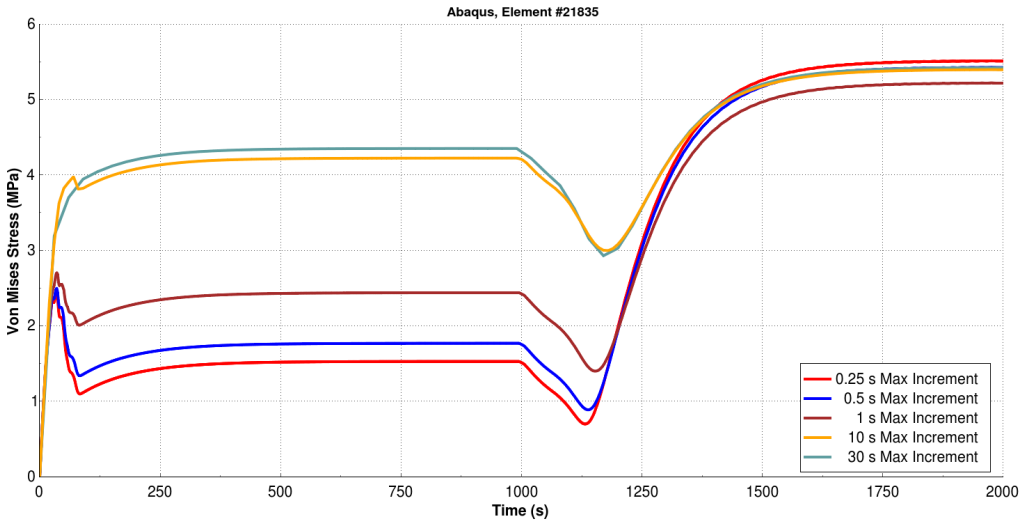

Figure 5.22: Convergence study, Abaqus, Von Mises Stress.

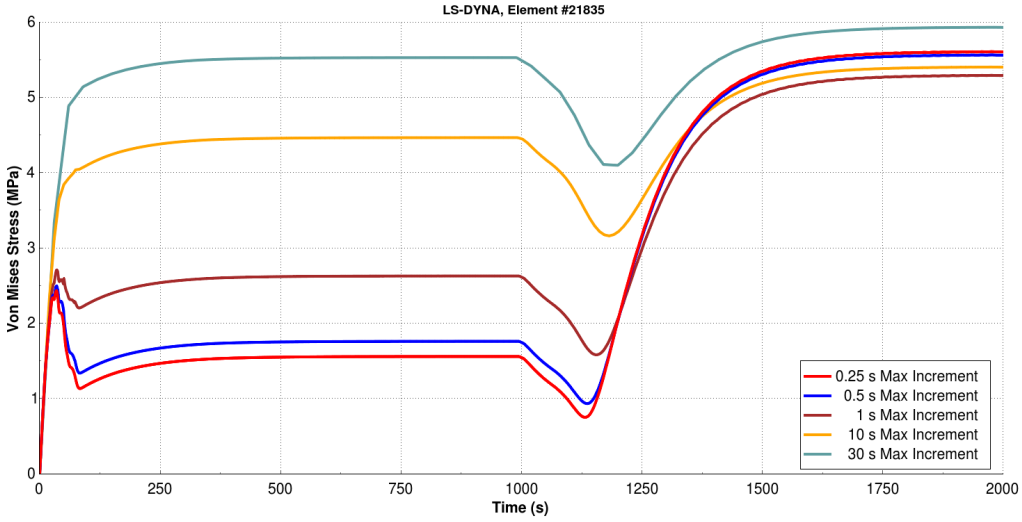

Figure 5.23: Convergence study, LS-DYNA, Von Mises Stress.

Worth noting from these results is that the results for the 10 s and 30 s maximum increment size were similar in magnitude in Abaqus, which was not the case for LS-DYNA. In both Abaqus and LS-DYNA, the largest variation in magnitude between the increment sizes occurred during the heating phase.

Furthermore, the largest residual stress in Abaqus was obtained for the 0.25 s maximum increment, whilst the largest residual stress in LS-DYNA was obtained for the 30 s maximum increment. As with the results for the displacement, where LS-DYNA with 0.5 s maximum increment was deemed an outlier, it is not entirely clear why the results for 30 s maximum increment diverged from the general trend. With that said, since all the results in the convergence study indicate that the results are strongly influenced by the increment size, and that the solution converges for a sufficiently small increment size, the results for the 30 s maximum increment size can in large be regarded as erroneous.

From the convergence study, it was observed that the time increment size had a major impact on all results. This trend was seen in both Abaqus and LS-DYNA, meaning that this is not correlated with the implementation of the material model in Abaqus, but rather connected to the subroutine umat42 in the object file obtained from RISE.

In both solvers, the results had converged with an increment size of around 0.25 s to 0.5, with significant differences for the larger increment sizes. In the applications where the material model is of interest at Volvo Cars, the increment size needs to be considerably larger than 0.5 s in order to have reasonable computational times. Therefore, the possibility to obtain accurate results for large models is somewhat restricted with the current implementation of the material model.

5.2 Comparison With Physical Test

This section will account for the results of the Hat Profile component. This includes the Abaqus simulations and a physical test.

5.2.1 Hat Profile

The vertical displacement of the lid from the test and the Abaqus simulation in the middle of the oven process, at a temperature of 185°C, can be seen in Figure 5.24. In the figure, the positive deformation is defined as out of the plane of the paper in both the physical test and the simulation, which corresponds to the negative y-direction in Abaqus, defined in Figure 4.10 in Section 4.3.1. The maximum increment size used in the Abaqus simulation was 30 s.

A note on the test results is that what looks like a “split” in the component is due to missing data in that particular region, since the 3D-scanning device could not reach this region as the component was placed in a fixture during the test.

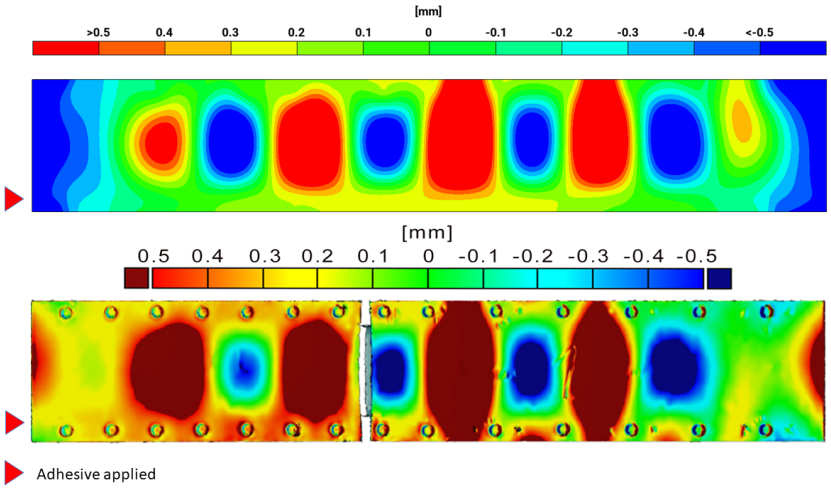

Figure 5.24: Vertical deformation of the lid at temperature 185°C. Top: Abaqus, Bottom: Test case.

The lid had similar local deformations when comparing the simulated results to the test, as it exhibited the same buckling behaviour in both cases. The exception was the two short edges, where the displacements were in opposite directions. A notable difference was the large deformations at the long side with adhesive applied in the test, which were due to adhesive failure, and therefore were not present in the simulation results.

The vertical deformations of the hat from the test and the Abaqus simulation can be seen in Figure 5.25. As in the previous figure, the positive direction is defined as out of the plane of the image, which in this case corresponds to the positive y-direction in Abaqus.

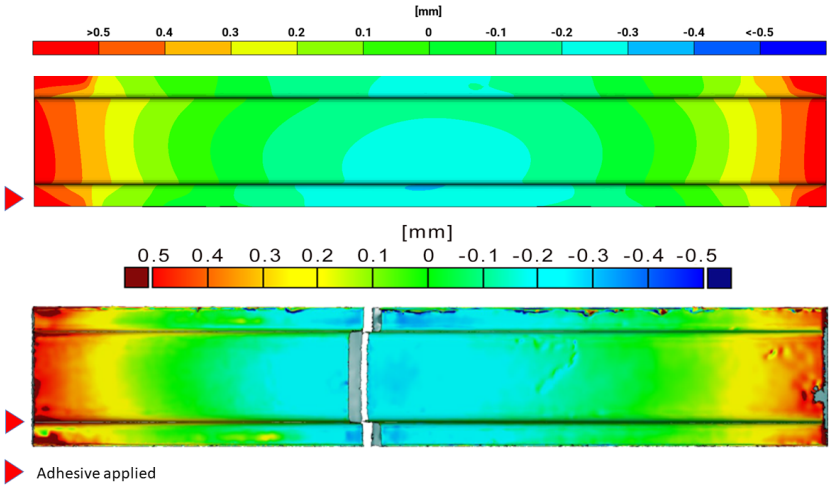

Figure 5.25: Deformation of Hat Profile on the top side at temperature 185°C. Abaqus: top, Test case: bottom.

It can be noted that the same global trend is apparent in both the simulation and test results, as the hat exhibited bending behaviour with both short edges displaced in the positive direction whilst the middle segment deformed in the negative direction. The hat had no significant local deformations in either the test or the simulation.

A further observation is that the there were some differences in the global deformations from the test results of the lid, seen in Figure 5.24, and the hat, seen in Figure 5.25, even though the parts were joined together. One possible explanation for this could be separation of the two parts due to the adhesive failure.

The residual deformations of the lid after cooling can be seen in Figure 5.26. The direction of the displacements is defined in the same manner as in Figure 5.24.

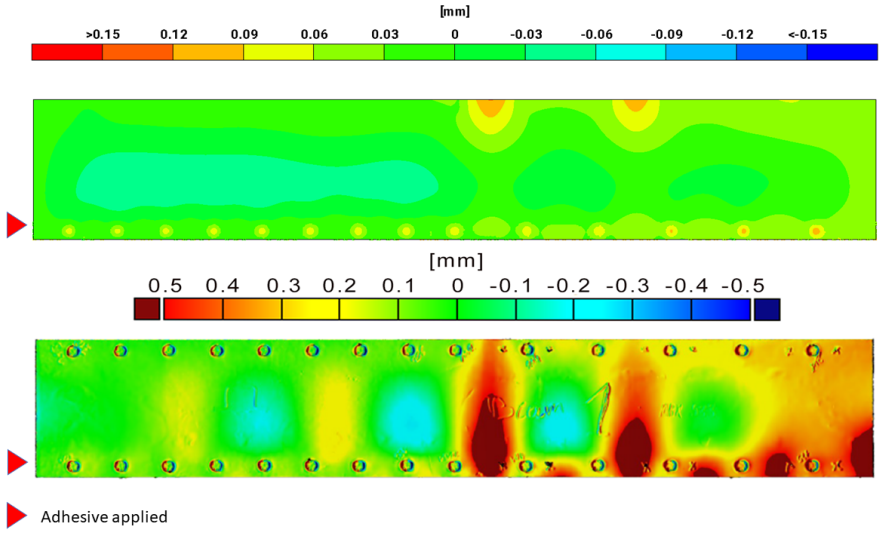

Figure 5.26: Residual deformations of the lid at temperature 20°C. Abaqus: top, Test case: bottom.

In the results for the residual displacement of the lid, it can be seen that the magnitudes of the displacements have decreased when compared to the displacements at 185 °C in Figure 5.24. This trend is apparent in the results from both the simulation and the test case.

With that said, the difference in magnitude between the test and the simulation was more apparent for the residual displacement when compared to the displacements at 185 °C. This was true both for the global and local deformations, where the residual deformations in some regions were 10 times higher in the test results compared to simulation results.

The differences noted between the simulation and the test were likely due to the adhesive failure in the test. This is apparent as the largest residual displacements in the test appeared on the side with adhesive applied, whilst it in the Abaqus simulation appeared on the side with no adhesive applied.

The error between the residual deformations on the lid also correlated with the results obtained from the convergence study of the Bi-Metal Strip in Figure 5.18, where large time increment sizes resulted in an underestimation of the residual displacement. Therefore, it could be reasoned that the residual displacement would match better with the test case if the maximum increment size was smaller than 30 s.

With that said, the purpose of the Hat Profile was to use the material model in a scenario relevant to future applications at Volvo Cars. In many of these applications, it will no be possible to use increment sizes smaller than $10 - 20$ s due to computational times, and it was therefore deemed more relevant to use a 30 s maximum increment in this case.

The residual displacement of the hat can be seen in Figure 5.27. In the figure, the positive direction of the displacements is defined as in Figure 5.25. In these results, it can be seen that the residual displacements of the hat were close to zero in both the Abaqus simulation and the test case.

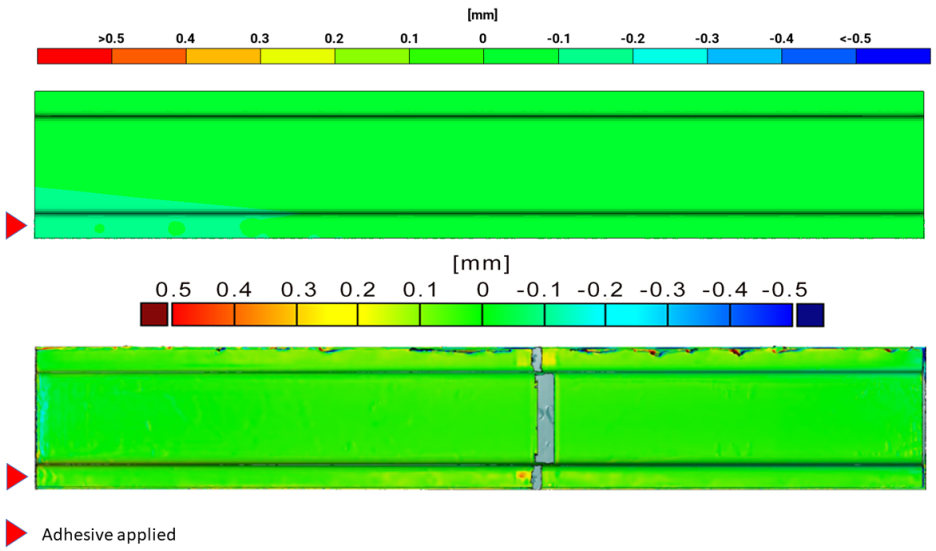

Figure 5.27: Residual deformation on the hat at temperature 20°C. Abaqus: top, Test case: bottom.

As in the results at 185 °C, the global trend for the hat and the lid did not match entirely. In Figure 5.26 it can be seen that right edge of the lid has deformations with a magnitude of approximately 0.5 mm, whilst in Figure 5.27, no apparent residual deformation can be seen.

To conclude the comparison between the test and the simulation of the Hat Profile, the same general trends were seen in both cases, although the difference in the residual deformation was more significant than the deformations at 185 °C.

To have a more representative comparison between simulation and test, either the

simulation model would have to be more complex and include the aspect of adhesive failure, or the test component would have to be designed in a way that limits the risk of adhesive failure. For the Hat Profile, one such design aspect is the rivet pitch, as no adhesive failure occurred with 40 mm pitch length, compared to the 60 mm pitch length, where significant adhesive failure occurred. A better representation could also be achieved by using a smaller maximum time increment size, as discussed previously.

6

Conclusion & Recommendation for Further Work

In both the case of the Single Element and the Bi-Metal Strip, the results between Abaqus and LS-DYNA were within the allowable error tolerance of 10%. In fact, the maximum relative error for the displacement was 6.80 % and the maximum relative error for the stress was 1.69 %. Thereby the main objective of the thesis, which was to implement the material model in Abaqus such that it gave the same results as in LS-DYNA, was fulfilled.

The discrepancies seen in the results for the Bi-Metal Strip were determined to have their root in the time increment size. The same trend was seen in both Abaqus and LS-DYNA, indicating that the issue was located in the subroutine obtained from RISE. This observation has been brought forward to RISE, and they are as of now working on resolving the issues.

Even though evaluating the validity of the material model was not in the scope of the thesis, it is for future work recommended that the implementation of the material model, and any updated versions of it, is validated against physical test cases in both LS-DYNA and Abaqus to validate both the implementation. Moreover, the same kind of evaluation as was performed in the convergence study in this thesis should be performed with an improved model. This is especially important since the applications in which the material model will be used at Volvo Cars require a significantly larger increment size than 0.5 s (at which the solution converged for the Bi-Metal Strip) to ensure reasonable computational times.

As can be seen in the physical test of the Hat Profile, the largest residual displacements were seen on the flange where adhesive had been applied. It would therefore be of interest to investigate the actual influence of the adhesive further.

A further recommendation for future work related to the Hat Profile results is the inclusion of adhesive failure in the material model, as this had a significant effect on the residual displacements of the component.

As of now, it is possible to use the implemented material model in Abaqus for smaller structures, as the computational time for the simulations is the restriction.

Therefore the main recommendation for further improvements of the implementation in Abaqus is to make it compatible with parallel execution. This improvement is necessary to run the desired simulations in Abaqus at Volvo Cars with reasonable computational times.

The second improvement of the Abaqus implementation that could be taken into consideration in further work is the initializing of the solution-dependant state variables within the subroutine. As of now, the subroutine uses the correct values in the calculations, but the results for the solution-dependant state variable output for time $t = 0$ are not accurate. This could possibly be achieved with the subroutine SDVINI. It should however be noted that the solution-dependant state variables are not of any particular interest at Volvo Cars. It is mainly the stress end displacement results that are of interest, and these results are not affected in any way.

In conclusion, it can be said that the overall aim of the thesis is fulfilled, but some improvements have to be made to use the adhesive material model for simulations of large structures. These improvements are moreover required in order to assure that the simulations yield accurate and reliable results. These improvements require participation from both RISE and Volvo Cars, since the source code has not been made available to Volvo Cars. The improvements are related to both the material model itself and the implementations in both Abaqus and LS-DYNA.

Bibliography

[1] Dimensional reasearch. "Managing automotive technology trends, a survey of automobile oem stakeholders." (2018), [Online]. Available: https://www.jabil.com/dam/jcr:4174aad8-c400-443d-9114-7cbab4893e29/managing-automotive-technology-trends-report-jabil.pdf (visited on 01/25/2022).

[2] Kunskapsportalen. "Modeling of adhesive bonding for multi-material design - madbond." (), [Online]. Available: https://kunskapsformedlingen.se/en/projects/modeling-of-adhesive-bonding-for-multi-material-design-madbond/ (visited on 01/25/2022).

[3] S. Saseendran, D. Berglund, and J. Varna, "Viscoelastic model with complex rheological behavior (VisCoR): incremental formulation, advanced manufacturing: Polymer & composites science," DOI: 10.1080/20550340.2019.1709010.

[4] FEICA, *Guidance FMI-EX-F04-012*. [Online]. Available: http://www.feica.eu.

[5] Permabond. "Strongest adhesives for bonding metal, glass & plastic." (2022), [Online]. Available: https://www.permabond.com/resource-center/strongest-adhesive/ (visited on 04/21/2022).

[6] MASTERBOND. "What is and epoxy adhesive?" (2022), [Online]. Available: https://www.masterbond.com/techtips/what-epoxy-adhesive (visited on 04/21/2022).

[7] V. Gold, Ed., *The IUPAC Compendium of chemical terminology*. Research Triangle Park, NC: International Union of Pure and Applied Chemistry (IUPAC), 2019.

[8] K. Hodd, "37 - epoxy resins," in *Comprehensive Polymer Science and Supplements*, G. Allen and J. C. Bevington, Eds., Amsterdam: Pergamon, 1989, pp. 667–699, ISBN: 978-0-08-096701-1. DOI: https://doi.org/10.1016/B978-0-08-096701-1.00178-6. [Online]. Available: https://www.sciencedirect.com/science/article/pii/B9780080967011001786.

[9] WEST SYSTEM. "Uncontrolled cure." (2022), [Online]. Available: https://www.westsystem.com/safety/uncontrolled-cure/ (visited on 04/21/2022).

[10] PERMABOND. "When adhesives exotherm." (2022), [Online]. Available: https://www.permabond.com/resource-center/adhesives-exotherm/ (visited on 04/21/2022).

[11] ——, "Two component epoxy adhesive mix ratio." (2022), [Online]. Available: https://www.permabond.com/resource-center/two-component-epoxy-adhesive-mix-ratio/ (visited on 04/21/2022).

[12] MASTERBOND. "Two component epoxy adhesives." (), [Online]. Available: https://www.masterbond.com/products/two-component-epoxy-adhesives (visited on 05/10/2022).

[13] ——, "How to properly store epoxy adhesives." (), [Online]. Available: https://www.masterbond.com/techtips/how-properly-store-epoxy-adhesives (visited on 05/10/2022).

[14] EPOXIES. "FreezeBond - Premixed & Frozen Epoxies." (2022), [Online]. Available: https://www.epoxies.com/products/freezebond/ (visited on 04/21/2022).

[15] PERMABOND. "Consistent Single Component Epoxy Curing." (2022), [Online]. Available: https://www.permabond.com/resource-center/consistent-single-component-epoxy-curing/ (visited on 04/22/2022).

[16] MASTERBOND. "One component epoxy adhesives." (), [Online]. Available: https://www.masterbond.com/products/one-component-epoxy-systems (visited on 05/10/2022).

[17] WEST SYSTEM. "Modifying with fillers & additives." (2022), [Online]. Available: https://www.westsystem.com/instruction-2/epoxy-basics/modifying-with-fillers-additives/ (visited on 04/22/2022).

[18] MASTERBOND. "Why use epoxy hybrid adhesives?" (2022), [Online]. Available: https://www.masterbond.com/techtips/why-use-epoxy-hybrid-adhesives (visited on 04/22/2022).

[19] J. Guillemenet, S. Bistac, and J. Schultz, "Relationship between polymer viscoelastic properties and adhesive behaviour," *International Journal of Adhesion and Adhesives*, vol. 22, no. 1, pp. 1–5, 2002, ISSN: 0143-7496. DOI: https://doi.org/10.1016/S0143-7496(01)00027-6. [Online]. Available: https://www.sciencedirect.com/science/article/pii/S0143749601000276.

[20] M. Girard *et al.*, "A simple characterization methodology for the identification of the visco-elastic behavior of thermoset adhesives during cure," *Applied Adhesion Science*, vol. 8, no. 1, p. 2, Feb. 2020, ISSN: 2196-4351. DOI: 10.1186/s40563-020-00125-4. [Online]. Available: https://doi.org/10.1186/s40563-020-00125-4.

[21] A. Takahashi, Y. Sekiguchi, and C. Sato, "Volume change and viscoelastic properties of uv-curable adhesives for precise positioning during curing process and their formulation," *The Journal of Adhesion*, vol. 0, no. 0, pp. 1–16, 2021. DOI: 10.1080/00218464.2021.1950538. eprint: https://doi.org/10.1080/00218464.2021.1950538. [Online]. Available: https://doi.org/10.1080/00218464.2021.1950538.

[22] Composites Knowledge Network (CKN). "Degree of cure - A104." (2021), [Online]. Available: https://compositeskn.org/KPC/A104 (visited on 03/04/2022).

[23] ——, "Cure of thermosetting polymers - A162." (2021), [Online]. Available: https://compositeskn.org/KPC/A162 (visited on 03/04/2022).

[24] M. R. Kamal, "Thermoset characterization for moldability analysis," *Polymer Engineering & Science*, vol. 14, no. 3, pp. 231–239, 1974. DOI: https://doi.org/10.1002/pen.760140312. eprint: https://onlinelibrary.wiley.com/doi/pdf/10.1002/pen.760140312. [Online]. Available: https://onlinelibrary.wiley.com/doi/abs/10.1002/pen.760140312.

[25] S. Schricker, "9 - composite resin polymerization and relevant parameters," in *Orthodontic Applications of Biomaterials*, T. Eliades and W. A. Brantley, Eds., Woodhead Publishing, 2017, pp. 153–170, ISBN: 978-0-08-100383-1. DOI: https://doi.org/10.1016/B978-0-08-100383-1.00009-6. [Online]. Available: https://www.sciencedirect.com/science/article/pii/B9780081003831000096.

[26] K. Priesnitz, "On local panel distortions due to hot-curing adhesives," Ph.D. dissertation, Delft University of Technology, 2015. [Online]. Available: https://repository.tudelft.nl/islandora/object/uuid:496c78af-cf05-47b6-a35a-20609202c169/datastream/OBJ/download.

[27] C. Li *et al.*, "In-situ measurement of chemical shrinkage of MY750 epoxy resin by a novel gravimetric method," *Composites Science and Technology*, vol. 64, no. 1, pp. 55–64, 2004, ISSN: 0266-3538. DOI: https://doi.org/10.1016/S0266-3538(03)00199-4. [Online]. Available: https://www.sciencedirect.com/science/article/pii/S0266353803001994.

[28] S. White and H. Hahn, "Process modeling of composite materials: Residual stress development during cure. part i. model formulation," *Journal of Composite Materials*, pp. 2402–2422, 1992. [Online]. Available: https://journals.sagepub.com/doi/10.1177/002199839202601604 (visited on 05/09/2022).

[29] M. S. Genidy, M. S. Madhukar, and J. D. Russell, "A new method to reduce cure-induced stresses in thermoset polymer composites, part ii: Closed loop feedback control system," *Journal of Composite Materials*, 2000. [Online]. Available: https://journals.sagepub.com/doi/10.1106/3M0Y-44XM-6WP8-WT7J (visited on 05/09/2022).

[30] M. A. Meyers and K. K. Chawla, *Mechanical behavior of materials*. Cambridge university press, 2008.

[31] S. A. Ashter, "7 - characterization," in *Thermoforming of Single and Multilayer Laminates*, S. A. Ashter, Ed., Oxford: William Andrew Publishing, 2014, pp. 147–192, ISBN: 978-1-4557-3172-5. DOI: https://doi.org/10.1016/B978-1-4557-3172-5.00007-4. [Online]. Available: https://www.sciencedirect.com/science/article/pii/B9781455731725000074.

[32] G. Papanicolaou and S. Zaoutsos, "1 - viscoelastic constitutive modeling of creep and stress relaxation in polymers and polymer matrix composites," in *Creep and Fatigue in Polymer Matrix Composites (Second Edition)*, ser. Woodhead Publishing Series in Composites Science and Engineering, R. M. Guedes, Ed., Second Edition, Woodhead Publishing, 2019, pp. 3–59, ISBN: 978-0-08-102601-4. DOI: https://doi.org/10.1016/B978-0-08-102601-4.00001-1. [Online]. Available: https://www.sciencedirect.com/science/article/pii/B9780081026014000011.

[33] M. A. Tapia-Romero, M. Dehonor-Gómez, and L. E. Lugo-Uribe, "Prony series calculation for viscoelastic behavior modeling of structural adhesives from DMA data," *Ingeniería, investigación y tecnología*, vol. 21, no. 2, 2020.

[34] LMS Technologies Vietnam. "Dynamic mechanical analysis (DMA/DMTA)." (2018), [Online]. Available: https://lmstech.com.vn/dynamic-mechanical-analysis-dmadmta (visited on 05/11/2022).

[35] NETZSCH. "Dynamic mechanical analysis (DMA)." (2022), [Online]. Available: https://analyzing-testing.netzsch.com/en/contract-testing/methods/dynamic-mechanical-analysis-dma (visited on 05/11/2022).

[36] Massachusetts Institute of Technology. "Time domain viscoelasticity." (2022), [Online]. Available: https://abaqus-docs.mit.edu/2017/English/SIMACAEMATRefMap/simamat-c-timevisco.htm (visited on 05/11/2022).

[37] B. Herzog *et al.*, "Glass-transition temperature based on dynamic mechanical thermal analysis techniques as an indicator of the adhesive performance of vinyl ester resin," *Journal of Applied Polymer Science*, vol. 97, no. 6, pp. 2221–2229, 2005. DOI: https://doi.org/10.1002/app.21868. eprint: https://onlinelibrary.wiley.com/doi/pdf/10.1002/app.21868. [Online]. Available: https://onlinelibrary.wiley.com/doi/abs/10.1002/app.21868.

[38] M. Mours and H. Winter, "Chapter 5 - mechanical spectroscopy of polymers," in *Experimental Methods in Polymer Science*, ser. Polymers, Interfaces and Biomaterials, T. Tanaka, Ed., Boston: Academic Press, 2000, pp. 495–546, ISBN: 978-0-08-050612-8. DOI: https://doi.org/10.1016/B978-0-08-050612-8.50011-8. [Online]. Available: https://www.sciencedirect.com/science/article/pii/B9780080506128500118.

[39] J. Bergström, "6 - linear viscoelasticity," in *Mechanics of Solid Polymers*, J. Bergström, Ed., William Andrew Publishing, 2015, pp. 309–351, ISBN: 978-0-323-31150-2. DOI: https://doi.org/10.1016/B978-0-323-31150-2.00006-6. [Online]. Available: https://www.sciencedirect.com/science/article/pii/B9780323311502000066.

[40] NETZSCH. "Williams-landel-ferry equation for master curve." (2022), [Online]. Available: https://analyzing-testing.netzsch.com/en/training-know-how/glossary/williams-landel-ferry-equation-for-master-curve (visited on 05/13/2022).

[41] V. Dorléans *et al.*, "Time-temperature superposition in viscoelasticity and viscoplasticity for thermoplastics," *Polymer Testing*, vol. 101, p. 107 287, 2021, ISSN: 0142-9418. DOI: https://doi.org/10.1016/j.polymertesting.2021.107287. [Online]. Available: https://www.sciencedirect.com/science/article/pii/S0142941821002361.

[42] P. Hajikarimi and F. Moghadas Nejad, "Chapter 5 - time–temperature superposition," in *Applications of Viscoelasticity*, P. Hajikarimi and F. Moghadas Nejad, Eds., Elsevier, 2021, pp. 83–105, ISBN: 978-0-12-821210-3. DOI: https://doi.org/10.1016/B978-0-12-821210-3.00006-1. [Online]. Available: https://www.sciencedirect.com/science/article/pii/B9780128212103000061.

[43] D. Ratna, "3 - thermal properties of thermosets," in *Thermosets*, Q. Guo, Ed., Woodhead Publishing, 2012, pp. 62–91, ISBN: 978-0-85709-086-7. DOI: https://doi.org/10.1533/9780857097637.1.62. [Online]. Available: https://www.sciencedirect.com/science/article/pii/B9780857090867500031.

[44] C. Obbink-Huizer. "Implicit vs explicit finite element analysis: When to use which?" (2017), [Online]. Available: https://info.simuleon.com/blog/implicit-vs-explicit-finite-element-analysis (visited on 04/07/2022).

[45] *LS-DYNA® theory manual*, Livermore Software Technology (LST), 7374 Las Positas Road, Livermore, California 94551, 2006, pp. 611–623. [Online]. Available: https://www.lstc.com/pdf/ls-dyna_theory_manual_2006.pdf.

[46] H. Hashamdar, Z. Ibrahim, and M. Jameel. "Finite element analysis of nonlinear structures with newmark method." (2011), [Online]. Available: https://academicjournals.org/article/article1380797968_Hashamdar%20et%20al.pdf (visited on 05/09/2022).

[47] *LS-DYNA® keyword user's manual, volume II - material models*, R13, Livermore Software Technology (LST), 7374 Las Positas Road, Livermore, California 94551, 2021, pp. 1832–1835.

[48] NETZSCH. "Williams-landel-ferry equation for master curve." (), [Online]. Available: https://analyzing-testing.netzsch.com/en/training-know-how/glossary/williams-landel-ferry-equation-for-master-curve (visited on 05/10/2022).

[49] Britannica. "Arrhenius equation." (2021), [Online]. Available: https://www.britannica.com/science/Arrhenius-equation (visited on 05/10/2022).

A

Material Constants in umat42

Table A.1: Material Constants (cm) Array

cm	Variable	Description
1	bulk	Material bulk modulus
2	shear	Material shear modulus
3	lambda	Lambda parameter in DiBenedetto equation
4	tg0	Uncured Tg (Tg at alpha=0)
5	tginf	Fully cured Tg (Tg at alpha=1)
6	xgel	Gel point of resin
7	fliq	Liquid fraction of resin in the beginning of analysis
8	frub	Rubbery/vitrified fraction of resin in the beginning of analysis
9	a1	Parameter A1 in Kamal model for DoC
10	a2	Parameter A2 in Kamal model for DoC
11	e1	Parameter E1 in Kamal model for DoC
12	e2	Parameter E2 in Kamal model for DoC
13	m	Parameter m in Kamal model for DoC
14	na	Parameter na in Kamal model for DoC
15	nb	Parameter nb in Kamal model for DoC
16	axmax	Parameter A in xmax equation
17	bxmax	Parameter B in xmax equation
18	cmax	Parameter C in xmax equation
19	restrtopt	Flag for restart analysis
20	vpflag	Flag for viscoplasticity
21		Unused
22		Unused
23		Unused
24		Unused

Table A.2: Additional Material Constants (cma) Array

cma	Variable	Description
1	GEx	Glassy Youngs modulus in X direction
2	GEy	Glassy Youngs modulus in Y direction
3	GEz	Glassy Youngs modulus in Z direction
4	Gprxy	Glassy Poisson's ratio in XY
5	Gpryz	Glassy Poisson's ratio in YZ
6	GPrxz	Glassy Poisson's ratio in XZ
7	GGxy	Glassy Shear modulus in XY
8	GGyz	Glassy Shear modulus in YZ
9	GGxz	Glassy Shear modulus in XZ
10	REx	Rubbery Youngs modulus in X direction
11	REy	Rubbery Youngs modulus in Y direction
12	REz	Rubbery Youngs modulus in Z direction
13	RPrxy	Rubbery Poisson's ratio in XY
14	RPryz	Rubbery Poisson's ratio in YZ
15	RPrxz	Rubbery Poisson's ratio in XZ
16	RGxy	Rubbery Shear modulus in XY
17	RGyz	Rubbery Shear modulus in YZ
18	RGxz	Rubbery Shear modulus in XZ
19		Unused
20		Unused
21		Unused
22		Unused
23		Unused
24		Unused
25	Ralpx	Rubbery CTE in X direction
26	Ralpy	Rubbery CTE in Y direction
27	Ralpz	Rubbery CTE in Z direction
28	Rbetax	Rubbery CCS in X direction
29	Rbetay	Rubbery CCS in Y direction
30	Rbetaz	Rubbery CCS in Z direction
31		Unused
32		Unused
33	Galpx	Glassy CTE in X direction
34	Galpy	Glassy CTE in Y direction
35	Galpz	Glassy CTE in Z direction
36	Gbetax	Glassy CCS in X direction
37	Gbetay	Glassy CCS in Y direction
38	Gbetaz	Glassy CCS in Z direction
39	terms	Number of terms in Prony series
40	taucrvid	Curve ID for tau_i terms in Prony series
41	picrvid	Curve ID for w_i terms in Prony series
42	tref	Reference time in cure shift factor
43	Tref	Ref. temp. in WLF equation for temp. shift factor
44	Erel	Fully relaxed Youngs modulus
45	c1	Parameter c1 in WLF equation
46	c2	Parameter c2 in WLF equation
47	gk	VE parameter
48	gk1	VE parameter
49	hk	VE parameter
50	hk1	VE parameter
51	d1	VE parameter
52	d2	VE parameter
53		Unused
54		Unused
55		Unused
56		Unused

B

History Variables

History Variable (hsv)	Parameter	Description
1	temper	Temperature
2	fliq (read from I/P card)	Liquid fraction
3	frub (read from I/P card)	Rubbery fraction
4	1-hsv(3)-hsv(2)	Check parameter
5	tg	Glass transition temperature
6	xc	Degree of cure
7	dtk/dt0	time step size
8	aTk0/aTk1	Temperature shift factor
9	aCk0/aCk1	Cure shift factor
10	gk0/gk1	Factor in VE model = 1
11	hk0/hk1	Factor in VE model = 1
12…17	Straink1 (1 to 6 respectively)	Strain in 6 directions
19…24	deps (1 to 6 respectively)	Strain increment in 6 directions
25…78	Sk0	VE memory terms
79…87	C(I,J)	Stiffness matrix components

Figure B.1: Table giving description and parameters of the history variables.

C

Abaqus UMAT subroutine

```
C######################################################################
C UMAT subroutine for adhesive material using material model
C developed by RISE
C
      SUBROUTINE UMAT(STRESS,STATEV,DDSDDE,SSE,SPD,SCD,
     1 RPL,DDSDDT,DRPLDE,DRPLDT,
     2 STRAN,DSTRAN,TIME,DTIME,TEMP,DTEMP,PREDEF,DPRED,CMNAME,
     3 NDI,NSHR,NTENS,NSTATV,PROPS,NPROPS,COORDS,DROT,PNEWDT,
     4 CELENT,DFGRD0,DFGRD1,NOEL,NPT,LAYER,KSPT,JSTEP,KINC)
C
      INCLUDE 'ABA_PARAM.INC'
C
      CHARACTER*80 CMNAME
      DIMENSION STRESS(NTENS),STATEV(NSTATV),
     1 DDSDDE(NTENS,NTENS),DDSDDT(NTENS),DRPLDE(NTENS),
     2 STRAN(NTENS),DSTRAN(NTENS),TIME(2),PREDEF(1),DPRED(1),
     3 PROPS(NPROPS),COORDS(3),DROT(3,3),DFGRD0(3,3),DFGRD1(3,3),
     4 JSTEP(4)
C
C############### End standard Header ############################

C
C Define variables, Set dimension for Prony Series with number of terms
C
      DIMENSION CM(24),CMA(56),CRVP(9),CRVT(9)
C
      INTEGER i, j
      REAL*8 ZERO
C
      parameter(ZER0=0.d0)
C-----------------------------------------------------------------
C Define material parameters from props
C
C PROPS(1)  - Bulk modulus
C PROPS(2)  - Shear modulus
C PROPS(3)  - Lambda
C PROPS(4)  - Uncured T_g
C PROPS(5)  - Fully cured T_g
C PROPS(6)  - Gel point
C PROPS(7)  - Liquid fraction
C PROPS(8)  - Rubbery fraction
C PROPS(9)  - A1 kamal
C PROPS(10) - A2 kamal
C PROPS(11) - E1 kamal
C PROPS(12) - E2 kamal
C PROPS(13) - m kamal
C PROPS(14) - na kamal
C PROPS(15) - nb kamal
C PROPS(16) - axmax
C PROPS(17) - bxmax
```

```
C PROPS(18) - cxmax
C PROPS(19) - flag for restart analysis
C PROPS(20) - flag for viscoplasticity
C PROPS(21) - Glassy Youngs modulus [GE] (x=y=z)
C PROPS(22) - Glassy Poisson's ratio [GPr] (xy=yz=xz)
C PROPS(23) - Glassy Shear modulus [GG] (xy=yz=xz)
C PROPS(24) - Rubbery Youngs modulus [RE] (x=y=z)
C PROPS(25) - Rubbery Poisson's ratio [RPr] (xy=yz=xz)
C PROPS(26) - Rubbery Shear modulus [RG] (xy=yz=xz)
C PROPS(27) - Rubbery CTE [Ralp] (x=y=z)
C PROPS(28) - Rubbery CCS [Rbeta] (x=y=z)
C PROPS(29) - Glassy CTE [Galp] (x=y=z)
C PROPS(30) - Glassy CCS [Gbeta] (x=y=z)
C PROPS(31) - Number of terms in Prony series
C PROPS(32) - Reference time in cure shift factor
C PROPS(33) - Reference temperature in WLF equation
C PROPS(34) - E_rel fully relaxed Young's modulus   (unused)
C PROPS(35) - c1 WLF
C PROPS(36) - c2 WLF
C PROPS(37) - gk
C PROPS(38) - gk1
C PROPS(39) - hk
C PROPS(40) - hk1
C PROPS(41) - d1
C PROPS(42) - d2
C-----------------------------------------------------------------
C
C CM (Material constants) Array
C
      do i = 1,24
        CM(i) = ZERO
      enddo
C
      do i = 1,20
        CM(i) = PROPS(i)
      enddo
C
C CMA (Aditional Material Constants) Array
C
      do i = 1,56
        CMA(i) = ZERO
      enddo
C
      CMA(1) = PROPS(21)
      CMA(2) = PROPS(21)
      CMA(3) = PROPS(21)
      CMA(4) = PROPS(22)
      CMA(5) = PROPS(22)
      CMA(6) = PROPS(22)
      CMA(7) = PROPS(23)
```

```
      CMA(8) = PROPS(23)
      CMA(9) = PROPS(23)
      CMA(10) = PROPS(24)
      CMA(11) = PROPS(24)
      CMA(12) = PROPS(24)
      CMA(13) = PROPS(25)
      CMA(14) = PROPS(25)
      CMA(15) = PROPS(25)
      CMA(16) = PROPS(26)
      CMA(17) = PROPS(26)
      CMA(18) = PROPS(26)
      CMA(25) = PROPS(27)
      CMA(26) = PROPS(27)
      CMA(27) = PROPS(27)
      CMA(28) = PROPS(28)
      CMA(29) = PROPS(28)
      CMA(30) = PROPS(28)
      CMA(33) = PROPS(29)
      CMA(34) = PROPS(29)
      CMA(35) = PROPS(29)
      CMA(36) = PROPS(30)
      CMA(37) = PROPS(30)
      CMA(38) = PROPS(30)
      CMA(39) = PROPS(31)
      CMA(42) = PROPS(32)
      CMA(43) = PROPS(33)
      CMA(44) = PROPS(34)
      CMA(45) = PROPS(35)
      CMA(46) = PROPS(36)
      CMA(47) = PROPS(37)
      CMA(48) = PROPS(38)
      CMA(49) = PROPS(39)
      CMA(50) = PROPS(40)
      CMA(51) = PROPS(41)
      CMA(52) = PROPS(42)
C
C Prony series
C
      do i = 1,9
        CRVP(i) = ZERO
        CRVT(i) = ZERO
      enddo
C
      CRVP(1) = 0.1548d0
      CRVP(2) = 0.0584d0
      CRVP(3) = 0.1174d0
      CRVP(4) = 0.2396d0
      CRVP(5) = 0.2185d0
      CRVP(6) = 0.0170d0
      CRVP(7) = 0.1016d0
```

```
      CRVP(8) = 0.0362d0
      CRVP(9) = 0.0196d0
C
      CRVT(1) = 1.0d-11
      CRVT(2) = 1.0d-10
      CRVT(3) = 1.0d-09
      CRVT(4) = 1.0d-07
      CRVT(5) = 1.0d-05
      CRVT(6) = 1.0d-04
      CRVT(7) = 1.0d-03
      CRVT(8) = 1.0d-02
      CRVT(9) = 5.0d-01
C
C Call the umat42 subroutine
C
C CM = cm = material constant array
C DSTRAN = eps = strain increment array
C STRESS = sig = stress component array
C STATEV = hsv = history variable
C DTIME = dt1 = time step size
C TIME = time = problem time
C TEMP = temper = Current temperature
C CMA = cma = additional material constants
C CRVP = Prony series weights
C CRVT = Prony series times
C
C
      call umat42(CM,DSTRAN,STRESS,STATEV,DTIME,
     1 TIME(2),TEMP+DTEMP,CMA,CRVP,CRVT)
C
C Initialize zero matrix for jacobian
C
      do i = 1,NTENS
        do j = 1,NTENS
          DDSDDE(i,j) = ZERO
        enddo
      enddo
C
C Set Jacobian=Stiffness matrix
C
      DDSDDE(1,1) = STATEV(79)
      DDSDDE(2,2) = STATEV(80)
      DDSDDE(3,3) = STATEV(81)
      DDSDDE(4,4) = STATEV(82)
      DDSDDE(1,2) = STATEV(83)
      DDSDDE(2,1) = STATEV(83)
      DDSDDE(1,3) = STATEV(84)
      DDSDDE(3,1) = STATEV(84)
      DDSDDE(2,3) = STATEV(85)
      DDSDDE(3,2) = STATEV(85)
```

```
      DDSDDE(5,5) = STATEV(86)
      DDSDDE(6,6) = STATEV(87)
C
      RETURN
      END

c    Start header
c     subroutine umat42(cm,eps,sig,hsv,dt1,time,
c     1           temper,cma,crvP,crvt)
c    End header
c
c        cm     -       material constants array (I/P) size 24
c        eps    -       strain increment array (I/P) size 6 following
c                       Voight notation
c        sig    -       stress component array (O/P) size 6 following
c                       Voight notation
c        hsv    -       history variables array (I/P and O/P) size 150
c        dt1    -       time step size in current increment (I/P)
c        time   -       Problem time (I/P)
c        temper -       Current temperature (I/P)
c        cma    -       additional material constants array (I/P) size 50
c        crvP   -       Prony series weights (I/P) array size is equal to
c                       number of Prony terms.
c                               OBS maximum number of Prony terms is limited to 9
c        crvt   -       Prony series times (I/P) array size is equal
c                       to number of Prony terms.
c                               OBS maximum number of Prony terms is limited to 9
```

D

Abaqus UMAT Variables

Variables to be defined

In all situations

DDSDDE(NTENS,NTENS)

Jacobian matrix of the constitutive model, $\partial \Delta\boldsymbol{\sigma} / \partial \Delta\boldsymbol{\varepsilon}$, where $\Delta\boldsymbol{\sigma}$ are the stress increments and $\Delta\boldsymbol{\varepsilon}$ are the strain increments. `DDSDDE(I,J)` defines the change in the `I`th stress component at the end of the time increment caused by an infinitesimal perturbation of the `J`th component of the strain increment array. Unless you invoke the unsymmetric equation solution capability for the user-defined material, Abaqus/Standard will use only the symmetric part of `DDSDDE`. The symmetric part of the matrix is calculated by taking one half the sum of the matrix and its transpose.

For viscoelastic behavior in the frequency domain, the Jacobian matrix must be dimensioned as `DDSDDE(NTENS,NTENS,2)`. The stiffness contribution (storage modulus) must be provided in `DDSDDE(NTENS,NTENS,1)`, while the damping contribution (loss modulus) must be provided in `DDSDDE(NTENS,NTENS,2)`.

STRESS(NTENS)

This array is passed in as the stress tensor at the beginning of the increment and must be updated in this routine to be the stress tensor at the end of the increment. If you specified initial stresses (Initial conditions in Abaqus/Standard and Abaqus/Explicit), this array will contain the initial stresses at the start of the analysis. The size of this array depends on the value of `NTENS` as defined below. In finite-strain problems the stress tensor has already been rotated to account for rigid body motion in the increment before `UMAT` is called, so that only the corotational part of the stress integration should be done in `UMAT`. The measure of stress used is "true" (Cauchy) stress.

If the `UMAT` utilizes a hybrid formulation that is total (as opposed to the default incremental behavior), the stress array is extended beyond `NTENS`. The first `NTENS` entries of the array contain the stresses, as described above. The additional quantities are as follows:

`STRESS(NTENS+1)`

Read only: $\widehat{J}$,

`STRESS(NTENS+2)`

Write only: $\widehat{K} = J\frac{\partial^2 U}{\partial \widehat{J}^2}$, and

`STRESS(NTENS+3)`

Write only: $\frac{\partial \widehat{K}}{\partial \widehat{J}} = J\frac{\partial^3 U}{\partial \widehat{J}^3}$, where U is the volumetric part of the strain energy density potential.

STATEV(NSTATV)

An array containing the solution-dependent state variables. These are passed in as the values at the beginning of the increment unless they are updated in user subroutines `USDFLD` or `UEXPAN`, in which case the updated values are passed in. In all cases `STATEV` must be returned as the values at the end of the increment. The size of the array is defined as described in Allocating space.

In finite-strain problems any vector-valued or tensor-valued state variables must be rotated to account for rigid body motion of the material, in addition to any update in the values associated with constitutive behavior. The rotation increment matrix, `DROT`, is provided for this purpose.

SSE, SPD, SCD

Specific elastic strain energy, plastic dissipation, and "creep" dissipation, respectively. These are passed in as the values at the start of the increment and should be updated to the corresponding specific energy values at the end of the increment. They have no effect on the solution, except that they are used for energy output.

Only in a fully coupled thermal-stress or a coupled thermal-electrical-structural analysis

RPL

Volumetric heat generation per unit time at the end of the increment caused by mechanical working of the material.

DDSDDT(NTENS)

Variation of the stress increments with respect to the temperature.

DRPLDE(NTENS)

Variation of RPL with respect to the strain increments.

DRPLDT

Variation of RPL with respect to the temperature.

Only in a geostatic stress procedure or a coupled pore fluid diffusion/stress analysis for pore pressure cohesive elements

RPL

RPL is used to indicate whether or not a cohesive element is open to the tangential flow of pore fluid. Set RPL equal to 0 if there is no tangential flow; otherwise, assign a nonzero value to RPL if an element is open. Once opened, a cohesive element will remain open to the fluid flow.

Variables that can be updated

PNEWDT

Ratio of suggested new time increment to the time increment being used (DTIME, see discussion later in this section). This variable allows you to provide input to the automatic time incrementation algorithms in Abaqus/Standard (if automatic time incrementation is chosen). For a quasi-static procedure the automatic time stepping that Abaqus/Standard uses, which is based on techniques for integrating standard creep laws (see Quasi-static analysis), cannot be controlled from within the UMAT subroutine.

PNEWDT is set to a large value before each call to UMAT.

If PNEWDT is redefined to be less than 1.0, Abaqus/Standard must abandon the time increment and attempt it again with a smaller time increment. The suggested new time increment provided to the automatic time integration algorithms is PNEWDT × DTIME, where the PNEWDT used is the minimum value for all calls to user subroutines that allow redefinition of PNEWDT for this iteration.

If PNEWDT is given a value that is greater than 1.0 for all calls to user subroutines for this iteration and the increment converges in this iteration, Abaqus/Standard may increase the time increment. The suggested new time increment provided to the automatic time integration algorithms is PNEWDT × DTIME, where the PNEWDT used is the minimum value for all calls to user subroutines for this iteration.

If automatic time incrementation is not selected in the analysis procedure, values of PNEWDT that are greater than 1.0 will be ignored and values of PNEWDT that are less than 1.0 will cause the job to terminate.

Variables passed in for information

STRAN(NTENS)

An array containing the total strains at the beginning of the increment. If thermal expansion is included in the same material definition, the strains passed into UMAT are the mechanical strains only (that is, the thermal strains computed based upon the thermal expansion coefficient have been subtracted from the total strains). These strains are available for output as the "elastic" strains.

In finite-strain problems the strain components have been rotated to account for rigid body motion in the increment before UMAT is called and are approximations to logarithmic strain.

DSTRAN(NTENS)

Array of strain increments. If thermal expansion is included in the same material definition, these are the mechanical strain increments (the total strain increments minus the thermal strain increments).

TIME(1)

Value of step time at the beginning of the current increment or frequency.

TIME(2)

Value of total time at the beginning of the current increment.

DTIME

Time increment.

TEMP

Temperature at the start of the increment.

DTEMP

Increment of temperature.

PREDEF

Array of interpolated values of predefined field variables at this point at the start of the increment, based on the values read in at the nodes.

DPRED

Array of increments of predefined field variables.

CMNAME

User-defined material name, left justified. Some internal material models are given names starting with the "ABQ_" character string. To avoid conflict, you should not use "ABQ_" as the leading string for CMNAME.

NDI

Number of direct stress components at this point.

NSHR

Number of engineering shear stress components at this point.

NTENS

Size of the stress or strain component array (NDI + NSHR).

NSTATV

Number of solution-dependent state variables that are associated with this material type (defined as described in Allocating space).

PROPS(NPROPS)

User-specified array of material constants associated with this user material.

NPROPS

User-defined number of material constants associated with this user material.

COORDS

An array containing the coordinates of this point. These are the current coordinates if geometric nonlinearity is accounted for during the step (see Defining an analysis); otherwise, the array contains the original coordinates of the point.

DROT(3,3)

Rotation increment matrix. This matrix represents the increment of rigid body rotation of the basis system in which the components of stress (STRESS) and strain (STRAN) are stored. It is provided so that vector- or tensor-valued state variables can be rotated appropriately in this subroutine: stress and strain components are already rotated by this amount before UMAT is called. This matrix is passed in as a unit matrix for small-displacement analysis and for large-displacement analysis if the basis system for the material point rotates with the material (as in a shell element or when a local orientation is used).

CELENT

Characteristic element length, which is a typical length of a line across an element for a first-order element; it is half of the same typical length for a second-order element. For beams and trusses it is a characteristic length along the element axis. For membranes and shells it is a characteristic length in the reference surface. For axisymmetric elements it is a characteristic length in the (r, z) plane only. For cohesive elements it is equal to the constitutive thickness.

DFGRD0(3,3)

Array containing the deformation gradient at the beginning of the increment. If a local orientation is defined at the material point, the deformation gradient components are expressed in the local coordinate system defined by the orientation at the beginning of the increment. For a discussion regarding the availability of the deformation gradient for various element types, see Deformation gradient.

DFGRD1(3,3)

Array containing the deformation gradient at the end of the increment. If a local orientation is defined at the material point, the deformation gradient components are expressed in the local coordinate system defined by the orientation. This array is set to the identity matrix if nonlinear geometric effects are not included in the step definition associated with this increment. For a discussion regarding the availability of the deformation gradient for various element types, see Deformation gradient.

NOEL

Element number.

NPT

Integration point number.

LAYER

Layer number (for composite shells and layered solids).

KSPT

Section point number within the current layer.

JSTEP(1)

Step number.

JSTEP(2)

Procedure type key (see Results file output format).

JSTEP(3)

1 if NLGEOM=YES for the current step; 0 otherwise.

JSTEP(4)

1 if current step is a linear perturbation procedure; 0 otherwise.

KINC

Increment number.

Department of Industrial and Materials Science
CHALMERS UNIVERSITY OF TECHNOLOGY
Gothenburg, Sweden
www.chalmers.se

CHALMERS
UNIVERSITY OF TECHNOLOGY